Chapter 1

Introduction

1.1 Background

Using the receiver-side digital signal processing (DSP) to adaptively compensate the transmission impairments, which includes the chromatic dispersion (CD), polarization mode dispersion (PMD), optical filtering effect, and fiber nonlinearities, is a promising technique for next generation long haul transmission since it alleviates the requirement for the optical dispersion compensating module (DCM) [1]. Among the various types of fiber impairments, the CD is the most essential one since it would still degrade the transmission performance even in a short-reach application like a local access network (LAN). Because typically the CD would linearly distort the optical signal phase instead of its amplitude, this impairment could be fully compensated for by properly rotating back the signal's distorted phase. A general issue of the receiver-side equalization would be the square-law nature of a photodiode which would convert the linear CD impact into a nonlinear distortion (and would also yield the PMD-induced power fading), therefore making the fully compensation extremely difficult. There are various solutions to the nonlinear photodiode depending on the used receiving methods: coherent and incoherent detection. We will introduce the two methods in the following two paragraphs and talk about how the transmission impacts can be compensated for after the nonlinear photodiode.

The coherent detected system uses one local oscillator (LO, typically it is a receiver-side laser.) as a reference to beat with the received signal [2]. When the power of LO is several orders of magnitude larger than the received signal (as is usually the case), the photodiode essentially functions as an optical mixer and retains the low frequency components after the photodiode. Such a mechanism down-converts the optical signal to a baseband electrical

signal, and both the optical amplitude and phase are directly transferred to the electrical amplitude and phase after the photodiode. The nonlinear terms contributed by the photodiode would be relatively small and could be ignored when the LO power is much larger than the received signal. The post processing can approximate the CD-induced phase distortions by comparing the training and received signal and then compensate the CD distortion. Thus, the CD could be fully compensated for and would not be a detrimental issue. However, the requirements for the narrow linewidth of a LO and the dynamic polarization controller (PC) increase the hardware and operation cost in a coherent system. The costly coherent system would be more suitable for an ultra-long haul transmission in which the trade-off between the performance and cost could be made.

For an incoherent system, there is only the photodiode appearing at the receiver without a LO. Due to the square-law nature of a photodiode, only the optical power can be transferred into electrical signal and thus the phase information of the optical signal is lost. The CD-induced distortion after the photodiode could still be mitigated through various nonlinear signal processing techniques like the maximum likelihood sequence estimation (MLSE) [3] or Voltera series estimation [4]. However, the residual CD impact would still seriously degrade the transmission performance after a mid-term fiber transmission (> 300 km) [5]. This issue seems to be solved by the recently proposed digital self-coherent (DSC) system [6]. In the DSC, two sets of optical delay interferometers (ODIs), five photodiodes and five analog to digital converters (DACs) are required at the receiver. The two ODIs and the followed four photodiodes are used to estimate the received optical phase and the other one photodiode is used for detecting the optical amplitude. With the optical phase and amplitude information the receiver can digitally reconstruct the optical signal and then compensate the CD using techniques similar to those used in a coherent system. However, the ODIs, photodiodes, and ADCs increase the hardware burden and cost at the receiver. Besides, the field-reconstruction technique enhances the computing complexity to the electrical DSP and its efficiency would

be limited especially when the optical signal to noise ratio (OSNR) is low. Therefore, a laudable goal would be to provide an alternative direct detection format which could fully compensate the CD distortion through post signal processing. Later we will introduce the optical orthogonal frequency division multiplexed (OFDM) system which could convert both the optical amplitude and phase into electrical signal and thus the CD could possibly be compensated.

Meanwhile, the spectra efficiency (SE) is also an interesting issue other than the transmission distance since using a more spectra-efficient format could help enhance the system capacity. The conventional on-off keying (OOK) format could not afford the increasing high demands for a larger capacity. Thus, various advanced modulation formats have been proposed 1: differential phase shift keying (DPSK) [7], 2: differential quadrature phase shift keying (DQPSK) [7], 3: amplitude and differential phase shift keying (ADPSK) [8], and 4: four-level amplitude shift keying (4ASK) [8]. Except the DPSK, the other formats carry 2 bits per symbol and have a doubled SE compared to the conventional OOK format. Typically, a better performance would be obtained with a price of more complex transmitters and receivers. The architectures of the transmitter and receiver and the operation principles will be introduced in Chapter 2. The issues of each format will also be discussed then.

Instead of using a higher level (higher SE) modulation format, there are some alternative techniques which use the limited optical bandwidth more efficiently. One of such techniques is the code division multiplexing (CDM) or called the code division multiple access (CDMA) [9]. This technique suggests all users sharing the same bandwidth and time duration to transmit their data, rather than assigning any specific wavelength and time slot for any specific user like in a conventional wavelength and time division multiplexing system (WDM and TDM) systems. To prevent the resources from being occupied by the in-active users, this technique exhibits a more spectrally-efficient usage and thus has a higher SE compared to the conventional WDM and TDM techniques. Besides, since the decoding process for CDMA

needs the corresponding codeword assigned to that data, it also provides a high security transmission which would benefit the financial or military transmission network. Unfortunately, the non-orthogonality of developed unipolar optical codes would inevitably limit the maximum number of active users in a network. Besides, the tuning speed and dynamic range of the encoder and decoder are still limited by the used fiber Bragg grating (FBG) and these are still the issues for an OCDMA system (while recently the micro-ring is proposed to be used for the en/decoder in OCDMA, we are not going to talk about this newly proposed scheme because it would be beyond the scope of this thesis). Couples of optical OCDMA systems will be introduced and explained more detaily in chapter 2.

1.2 Motivation

This dissertation is motivated by the following issues pointed out in Section 1.1.

(i) A direct detected system which could retain both the optical amplitude and phase information after the nonlinear photodiode is imperatively required for a DSP-assisted long haul transmission. The direct detected optical orthogonal frequency division multiplexing (DD-OFDM), which modulates the data onto lots of narrow-bandwidth subcarriers, can achieve the above requirement and thus is suitable for a long-term transmission. The current issues, which are focused on in this dissertation, include how to modulate an OFDM signal more efficiently and how to keep all the linear optical impairments from transmitter to receiver still linear to the signal after the photodiode.

(ii) As a high level (> 1 bit/symbol) modulation format, the optical DQPSK is well known for its superior performance such as its robustness to the CD and PMD tolerances. However, the requirement for a complex transmitter and receiver limit the DQPSK system to be applied in a field industry. Facing this issue we could either simplify the

transmitter and receiver for the DQPSK format, or develop an alternative format with a similar performance but a simpler hardware implementation.

(iii) The non-orthogonality of the optical codes limits the maximum number of active users in an OCDMA LAN. In addition, a simple and compact en/decoder would be very helpful in an OCDMA-LAN. The other proposals in this dissertation include the development of OCDMA light source and the reduction of multiple access interference (MAI) to increase the number of active users.

1.3 Organization of the Dissertation

In chapter 1, the issues of DSP-assisted transmission, modulation formats and OCDMA systems are pointed out and the motivations trying to solve these issues are given. In chapter 2, an overview of various modulation formats, which includes DPSK and DQPSK, and multiplexing schemes such as OFDM and optical code division multiplexing (OCDM) are illustrated. In chapter 3, we introduce our proposed two types of direct detected optical OFDM formats: RF tone assisted OFDM and virtual single sideband OFDM (VSSB-OFDM). Their transmission performances are both theoretically evaluated and experimentally demonstrated.

In chapter 4, we demonstrate the generations of various modulation formats, such as DQPSK and ASK/RZ-DPSK labeled signals, by using one Dual-Drive MZM (DD-MZM). We also give some theoretical investigations to see more details into the optical spectra and bit error rate performance. Besides, we analyze the quantum limit of a 4-level ASK signal to indicate its potentially optimum performance, and then we provide a newly proposed phase modulated 4-level ASK (PM4ASK) format which has better CD, PMD, and optical filtering tolerances compared to the conventional 4ASK. In chapter 5, we propose a cost-effective

OCDMA light source using a self-injected Fabry-Pérot laser diode (FP-LD) combined with a FBG array. In additoin, we provide a frequency interleaved multi-group approach that mitigates the multiple access interference (MAI) inherently in an optical fast frequency hopping CDMA (OFFH-CDMA) system, and we also demonstrate the first optical multi-carrier CDMA (OMC-CDMA) system.

Finally, the summaries and future works are given in Chapter 6.

References:

[1] H. Bulow, F. Buchali, and A. Klekamp, "Electronic dispersion compensation," *IEEE J. Lightwave Technol.*, vol. 26, pp. 158-167, 2008.

[2] C. Wree, S. Bhandare, D. Becker, D. Mohr, A. Joshi, "Repeaterless 10.7-Gb/s DPSK Transmission Over 304 km of SSMF Using a Coherent Receiver and Electronic Dispersion Compensation," *IEEE Photon. Technol. Lett.*, vol. 20, pp. 407-409, 2008.

[3] G. Bosco, V. Curri, E. Roffe, P. Poggiolini, "Joint Effect of MLSE and Receiver Filters Optimization on Dispersion Robustness of IMDD, DPSK, DQPSK, and Duobinary Modulation," *IEEE Photon. Technol. Lett.*, vol. 19, pp. 2003-2005, 2007.

[4] X. Zhu, S. Kumar, S. Raghavan, Y. Mauro, and S. Lobanov, "Nonlinear Electronic Dispersion Compensation Techniques for Fiber-Optic Communication Systems," OFC'08, Paper JWA56.

[5] G. Bosco and P. Poggiolini, "Long-distance effectiveness of MLSE IMDD receivers," *IEEE Photon. Technol. Lett.*, vol. 18, pp. 1037-1039, 2006.

[6] X. Liu, S. Chandrasekhar, A. Leven, "Digital self-coherent detection," Optics Express, vol. 16, pp. 792-803, 2008.

[7] A. H. Gnauck, P. J. Winzer, "Optical phase-shift-keyed transmission," *IEEE J. Lightwave Technol.*, vol. 23, pp. 115-130, 2005..

[8] Y. Han and Guifang Li, "Theoretical sensitivity of direct-detection multilevel modulation formats for high spectral efficiency optical communications," *IEEE J. Selected Topics in Quantum Electronics*, vol. 12, pp. 571-580, 2006.

[9] A. E. Willner et al, "Advanced Techniques to Increase the Number of Users and Bit Rate in OCDMA Networks," *J. Selected Topic Quantum Electron.*, vol. 13, pp. 1403-1414, 2007.

Chapter 2

Overviews of Modulation and Multiplexing Techniques

2.1 Introduction

In this chapter, we will give the brief overviews for techniques including 1: optical orthogonal frequency division multiplexing (OFDM), 2: advanced modulation formats, and 3: optical code division multiplexing or multiple access (OCDM or OCDMA). For each topic, the previous approaches are presented and discussed, and then followed by issues which have not been solved yet.

The purposes of this chapter are two folded: (i) the introduction to these techniques and (ii) the motivations for this dissertation.

2.2 Optical Orthogonal Frequency Division Multiplexing

The fundamental of OFDM is illustrated in Fig. 2.1. The input binary data is firstly mapped onto QAM symbols, then zero-padded into a size of a power of 2 and transferred into time domain waveform through an inverse fast Fourier transform (IFFT). Typically a cyclic prefix is inserted between the adjacent OFDM blocks to provide a margin for synchronization and inter-block interference (IBI). The output waveform of an OFDM signal would be semi-Gaussian distributed, especially when the IFFT size is very large. The spectrum of the output waveform is shown in the inset of Fig. 2.1. The orthogonal nature of an OFDM system makes overlapping among data subcarriers possible since at the receiver these in-band interferences can be completely removed through the use of fast Fourier transform (FFT). It is these overlapping subcarriers that make an OFDM system more spectra-efficient.

At the receiver side, we remove the cyclic prefix, conduct the fast Fourier transform (FFT), and do the channel estimation and equalization to the received signal. Due to the

inherent nature of carrying information on many narrow bandwidth subcarriers, the equalization can be implemented by just multiplying a complex coefficient to the received data symbol. Such a simple equalization approach is famous in OFDM and is called the "one-tap equalizer".

Depending on the receiving techniques, optical OFDM can be divided into two categories: 1. Coherent Detection, and 2. Direct Detection.

2.2.1 Coherent Detection

Coherent optical OFDM, firstly proposed in [1], has superior transmission performance because both the CD and PMD effects can be compensated for by the receiver-side equalization [1-2].

Shown in Fig. 2.2 are the transmitter and receiver architectures of a coherent optical OFDM (CO-OFDM) system. The OFDM transmitter is essentially the same as the one described in Fig. 2.1 and its two outputs, i.e. the real and imaginary parts, are fed into the two arms of an optical I/Q modulator which is typically used for DQPSK signal generation [3]. The I/Q modulator functions as a optical mixer to up-convert the complex baseband OFDM signal to the real valued optical OFDM signal. The output signal is then field modulated onto an optical carrier and thus the optical OFDM signal is generated.

At the receiver, a local oscillator (LO) performed by a laser is used as a phase reference to the received signal. The transmitted signal combined with the LO passes through an optical hybrid [4], and the four output are fed into 2 pairs of balanced detectors. Due to the nature of the optical hybrid, the outputs of the balanced detectors are corresponding to the real (R) and imaginary parts of the received optical signal, and therefore both the optical amplitude and phase are retained after the photodiodes. After digitally sampled by the analog to digital converters (ADCs), the related post-processing at the receiver includes the synchronization, serial to parallel conversion (S/P), cyclic prefix removal, fast Fourier transform (FFT), and

equalization, which has been explained in Fig. 2.1.

Transmission of 1000 km uncompensated standard single mode fiber (SMMF) of a CO-OFDM signal has been demonstrated in [5]. Later a 4160 km transmission with a 25.8 Gbps CO-OFDM is delivered by Jansen in [6], and followed by a 16x52.6 Gbps WDM-OFDM system in [7].

Recently, polarization division multiplexing (PDM) has re-attracted much attention since the detrimental adaptive polarization controller typically required in a conventional coherent system can be alleviated by using the polarization diversity receiving combined with the post signal processing. The general PDM transmitter and receiver are depicted in Fig. 2.3(a) and (b). At the transmitter, two optical modulators for independently modulating the x- and y-polarization data are required before their outputs are combined by a following polarization beam combiner (PBC). At the receiver, the polarization diversity is used allowing the two data streams on the two polarizations get separated from each other by post signal processing. The combinations of PDM, coherent receiving, and signal processing make all the linear fiber impairments, such as the CD, PMD, and filtering effects, can be compensated for. The principle of data recovering of a PDM system can be simply described as follows. Assuming the transmitted data on two polarizations are x(k) and y(k) and the received signals of the two polarizations at the PBS outputs are p(k) and q(k), we can relate the [x(k), y(k)] to [p(k),q(k)] as

$$\begin{bmatrix} p(k) \\ q(k) \end{bmatrix} = \begin{bmatrix} H_{11} & H_{12} \\ H_{21} & H_{22} \end{bmatrix} \begin{bmatrix} x(k) \\ y(k) \end{bmatrix}$$

Using the least square or least mean square approach, we can get the channel matrix H which contains the CD, PMD and filtering information. Then the received signals are equalized by a matrix R which is the inverse of H:

$$\begin{bmatrix} x(k) \\ y(k) \end{bmatrix} = \begin{bmatrix} R_{11} & R_{12} \\ R_{21} & R_{22} \end{bmatrix} \begin{bmatrix} p(k) \\ q(k) \end{bmatrix}$$

Thus, without the requirement for a fast tracking polarization controller in the receiving end,

the PDM-OFDM system could double the system capacity by incorporating the polarization diversity and the post signal processing.For further information about the PDM-OFDM system, readers are referred to the reference [8].

Although the CO-OFDM now is a serious candidate for optical transmission, there are couples of issues including: 1. an extra local oscillator with a narrow linewidth is required. 2. The need for additional frequency offset and phase noise compensation at the receiver. 3. More complex optical hardware implementations for the receiver like the optical hybrids and balanced detectors. Although the CO-OFDM system requires more complex architectures, its superior transmission performance makes it a serious candidate for the future ultra-long haul transmission. However, for a medium transmission distance like in a metro-politan network, we need to find a more suitable transmission system which could relax the receiver-side hardware burdens inherently in a coherent OFDM system.

2.2.2 Direct Detection

The direct detection OFDM (DD-OFDM) is kind of different from CO-OFDM since conventionally the optical phase is lost due to the square-nature of the photodiode. The most intuitive solution to DD-OFDM is the power-modulated OFDM [9], which basically is yielded from the radio over fiber (RoF) system. The transmitted data is double sideband modulated on the optical power instead of optical field and thus at the receiver the signal can be recovered directly through one photodiode. However, the CD induced fading inherently existed in a double sideband system would strongly limit its transmission reach and thus makes this signal only suitable for a short reach transmission such as in a local access network (LAN).

To further enhance the transmission distance, a single sideband (SSB) format combined with the power-modulated OFDM has been suggested combating the CD induced fading [10]. Unfortunately, this power-modulated SSB-OFDM signal modulates the signal at the

quadrature point of MZM, therefore suffering the design tradeoff between the better CD tolerance and the sensitivity. Besides, the nonlinearity of the MZM limits the maximum achievable optical modulation index (OMI) and thus gives a worse sensitivity to this power-modulated SSB-OFDM system [11]. Recently, Lowery et al has proposed a field modulated SSB-OFDM to eliminate the nonlinearity problem in a power modulated SSB-OFDM system. This technique biases the MZM at a point near the null to control its optimum relative power of the optical carrier and the bearing signal. Due to the field modulation, a gap with the same bandwidth as the signal which is allocated in between the optical carrier and the signal is required to separate the signal-signal beat interference (SSBI) and the signal. The first direct detection field modulated SSB-OFDM has been transmitted over 400 km SSMF in [12]. The authors further propose three different kinds of field modulated SSB-OFDM [12] and they are depicted in Fig. 2.4. Fig. 2.4(a) shows the DD-OFDM transmitter using Hermitian symmetry and an optical filter. The required sampling rate of the digital to analog converter (DAC) is four times of the optical bandwidth. Fig. 2.4(b) shows another approach using up-conversion and an optical filter. The required DAC sampling rate is exactly the same as the output signal bandwidth and thus is the most spectrally-efficient technique. Fig. 2.4(c) shows the other architecture which uses a frequency domain Hilbert transform. This architecture, similar to the first approach, also requires the DAC with a sampling rate four times the signal bandwidth, but it alleviates the optical filter after the modulator (colorless). Since the sampling rate of the DAC is very critical for a high speed (>=10Gbps) transmission, the second approach which requires the least bandwidth of the DAC would be the most promising technique for DD-OFDM. The required OSNR for a BER of 10^{-3} is ~ 17 dB/ 0.1 nm in a 4 QAM format. Transmission of 1000 km SSMF using this format with 8 WDM channels has been demonstrated in [13]. However, there are some issues in this technique: 1. Extra RF components such as RF power amplifiers, synthesizers, and RF mixer are required. 2. The imperfections of the RF electronics (like the nonlinearity or

the un-sufficient bandwidth) would induce additional penalty to the transmitted signal.

2.3 Advanced Modulation Formats

There is a great trend to increase the fiber capacity during the past few years. Advanced modulation formats other than the conventional OOK format are developed and experiment demonstrated. In the following bunches of sub-sections we will introduce some robust transmission and spectrally efficient formats which have been proposed in recent years.

2.3.1 Differential Phase Shift Keying (DPSK)

The transmitter and receiver of an optical DPSK system are illustrated in Fig. 2.5 [14]. The electrical binary signal is firstly pre-coded and sent into the MZM biased at the null point. The binary data of 0 and 1 are encoded onto the optical phase as 0 and π, respectively. At the receiver, an optical delay interferometer (ODI) before the photodiode is used to convert the phase modulated signal into OOK format. There are basically two types of receiver: the single-ended detection and balanced detection. For the single-ended detection, the performance is similar to the OOK format while for balanced detection the inherent sensitivity (defined as the required optical signal to noise ratio to achieve a BER of 10^{-9}) can be improved by ~ 3 dB compared to OOK. This 3-dB gain means an approximately doubled maximum transmission distance if we consider only a linear system. In addition to this benefit of 3-dB gain, the constant power transmission of DPSK also makes it more tolerant to the fiber nonlinearities and thus it can enlarge the input power per span and reduce the number of optical amplifiers. Due to the above listed couples of advantages, the DPSK format actually is proposed and ready for industry application.

2.3.2 Differential Quaternary Phase Shift Keying (DQPSK)

In a DPSK system the signal is only modulated onto optical phase 0 and π. If we further

modulate the signal onto four optical phases with {0, π/2, π, 3π/2}, the modulated signal carries 2 bits/symbol and is called differential quadrature phase shift keying (DQPSK) format [14]. The typical transmitter and receiver for optical DQPSK formats are depicted in Fig. 2.6.

Shown in Fig. 2.6(a) is the DQPSK transmitter which consists of the two parallel DPSK modulators with the lower branch π/2 phase delay relative to the upper one. Since the DQPSK signal is phase modulated the output is still with a constant power which is similar to the DPSK signal. The receiver shown in Fig. 2.6(b) uses two ODIs to convert the constant-enveloped DQPSK signal into two streams of OOK signals which correspond to the in-phase (I) and quadrature-phase (Q) signal before the optical input being sent into the photodiodes [14]. The OSNR penalty of DQPSK is ~ 2 dB compared to the DPSK due to the shorter distance between the adjacent data symbols.

2.3.3 Other Four-Level Modulation Formats

Shown in Fig. 2.7 is the transmitter and receiver for a ASK/DPSK (ADPSK) format combining the DPSK and ASK with 2 bits per symbol. The modulation for ADPSK is very straightforward: one DPSK modulator firstly encodes the binary input data 1 on optical phase and the followed ASK modulator encodes the binary data 2 on optical power. At the receiver, the signal is split into two branches: one for ASK detection and other for differential phase detection. The finite extinction ratio (ER) for the ASK data is very critical to the signal performance [15]. With the same spectra efficiency (SE) as DQPSK, ADPSK saves one ODI and balanced receiver at the receiving end and therefore is with a lower cost. The issues of ADPSK include 1: the worse sensitivity compared to DQPSK (~2 dB) [15], and 2: the optimum ER of the ASK data strongly depends on the bandwidth of optical filter and the suffered CD effect [15], thus making the system difficult to optimize.

The simplest 4-level optical format would be the 4-level ASK (4ASK) [15-17] with its transmitter and receiver shown in Fig. 2.8. The two independent electrical signals with

different amplitudes are firstly summed into one 4-level ASK electrical signal. The 4–level ASK electrical signal is then converted into optical 4ASK signal by an optical ASK modulator. Only one photodiode is used for converting this 4ASK signal into 4 ASK electrical signal. The additional cost would be the requirement for a multi-level decision circuit. This simple format has the following issues: 1 the worse sensitivity due to the efficiency detection of multi-level detection (~5 dB), 2: the optimum level spacing depends on optical filtering and CD effects.

2.3.4 Performance Analysis for Modulation Formats

There are lots of published works regarding to performance analysis for modulation formats. Since the detailed explanation of each of them is lengthy, we only provide references here for these analysis tools.

1. *Optical spectral analysis.* Interested readers are referred to [18] for NRZ only and [19] for ideal RZ format (Please note that the "ideal" means the authors did not consider the rise-fall time of the data signal). Of course, you can also apply these algorithms to general RZ-OOK/RZ-DPSK/RZ-DQPSK formats after some manipulations.
2. *Karhunen-Loeve series expansion (KLSE).* KLSE is well-known for the noise modeling with least number of orthogonal functions. Facing the filtered Chi^2-distributed noise, people use the KLSE to derive the moment generating functions (MGFs) of both the signal and the noise, and then use the MGFs to evaluate the exact bit error rate in a system with arbitrary types of optical and electrical filters. Essentially there are two methods modeling the noise and the signal. They are: (i) the frequency-domain modeling [20] and (ii) the time-domain modeling [21]. The bit error rate or power penalty calculated in this dissertation uses time-domain modeling. However, the frequency-domain modeling would actually be more time-efficient.
3. *Saddle point approximation.* Interested readers are referred to [22]. This method can

simplify the BER evaluation while it can still maintain a good BER approximation.

4. *Quantum limit [15].* "The quantum limit, the ideal performance for a given class of optical receivers and a given modulation format, is defined as the minimum number of photons per bit required on average at the receiver input to obtain a certain bit error probability, most frequently BEP = 10^{-9}" [23]. This limit informs people which format would yield the best sensitivity and how much the relative penalties are among them. Conditions for quantum limit, (i) Use ideal input data (memoryless and no distortion). (ii) Use optical integrate and dump filter (optical matched filter). (iii) No post detection filter.

2.4 Optical Code Division Multiplexing

The general transmitter and receiver of an OCDMA system are depicted in Fig. 2.9. The input typically is a modulated short pulse data train. The data pulse train is fed into a specially designed fiber Bragg grating (FBG) to encode the modulated data with its own pattern, or more normally codeword. Depending on how the codeword is encoded onto the data pulse train, there are mainly three types of OCDMA:

2.4.1 Direct-sequence CDMA (DS-CDMA) [Fig. 2.9(a)].

The encoder is a super-structured FBG (SSFBG) with its spatial index distribution the same as the codeword [24]. Such a SSFBG would yield an encoded output waveform with the same time-domain pattern as the assigned codeword and thus can be used as a high speed passive encoder. Other than using the unipolar codes with a poor capacity, the combination of the DPSK and CDMA is proposed as a new scheme which uses the bipolar codes and thus can increase the system capacity [25]. The issue for unipolar or bipolar codes is that a weakly coupled SSFBG should be used for a better encoding performance, therefore inducing a significant power loss.

2.4.2 Fast frequency hopping CDMA (FFH-CDMA) [26-27].

The encoder used for FFH-CDMA is the cascaded FBGs with different reflected wavelengths. The relative positions of the FBGs depend on the pattern of the assigned codeword and the number of FBGs is determined by the length of codeword. The round trip time between two adjacent FBGs is equal to the chip duration. The encoded output waveform is shown in Fig. 2.9(b). The sequence of the colored pulses is determined by the assigned codeword. The time spacing between two colored pulses is defined as the chip duration, which is equal to the round trip time between two adjacent FBGs in the encoder. At the receiver, another FBG array (FBGA) reverse to the transmitter's FBGA is used for decoding the data. The decoded waveform shown at the receiver is the auto-correlation peak surrounded by the side-lobes. These side-lobes are caused by using the unipolar codes and would contribute significant interferences when the number of active users is large. This multiple access interference (MAI) is a serious issue when designing the FFH-CDMA system. Please note that the general version of FFH-CDMA includes the 2-dimensional CDMA (2D-CDMA) in which we insert some blank chips (no power transmitted on those chips) to enhance its security for transmission [28].

2.4.3 Spectra-encoding CDMA (SE-CDMA) [29].

The different wavelength components of the broadband coherent short pulse data are phase encoded by $\{0, \pi\}$. The encoded waveform looks like a random signal constrained within one bit duration as shown in Fig. 2.9(c). At the receiver, the output of decoder has one auto-correlation peak accompanied by side-lobes which is a result of the imperfections of encoder or decoder. The MAI can be virtually removed through the use of a balanced detector. The issue of this technique is the requirement for the free space en/decoding process which would result in a bulky en/decoder.

Reference

[1] W. Shieh and C. Athaudage, "Coherent optical orthogonal frequency division multiplexing," *Electron. Lett.*, vol. 42, pp. 587–589, 2006

[2] W. Shieh, "PMD-Supported Coherent Optical OFDM Systems," *IEEE Photon. Technol. Lett.*, vol. 19, pp. 134-136, 2007.

[3] A. H. Gnauck, P. J. Winzer, "Optical phase-shift-keyed transmission," *IEEE J. Lightwave Technol.*, vol. 23, pp. 115-130, 2005.

[4] T. G. Hodgkinson, R. A. Harmon, D. W. Smith, and P. J. Chidgey, "In-phase and quadrature detection using 90° optical hybrid receiver: experiments and design considerations," *IEE Proceedings J. Optoelectron.,* vol. 135, pp. 260-267, 1988.

[5] W. Shieh, X. Yi, Y. Tang, "Experimental Demonstration of Transmission of Coherent Optical OFDM Systems," OFC'2007, Paper OMP2.

[6] S. L. Jansen, I. Morita, T. C. W. Schenk, N. Takeda and H. Tanaka, "Coherent Optical 25.8-Gb/s OFDM Transmission Over 4160-km SSMF," *IEEE J. Lightwave Technol.*, vol. 26, pp. 6-15, 2008.

[7] S. L. Jansen, I. Morita, and H. Tanaka, "16x52.5-Gb/s, 50-GHz spaced, POLMUX-CO-OFDM transmission over 4,160 km of SSMF enabled by MIMO processing," ECOC2007, Paper PD 1.3.

[8] Y. Ma, W. Shieh, Q. Yang, "Bandwidth-Efficient 21.4 Gb/s Coherent Optical 2×2 MIMO OFDM Transmission," OFC2008, Paper JWA59.

[9] D. F. Hewitt et al, "Performance and applications of gigabit OFDM over optical fiber systems in metro and access networks," ECOC2006, Paper We3.

[10] M. Schuster, S. Randel, C. A. Bunge, S. C. J. Lee, F. Breyer, B. Spinnler and K. Petermann, "Spectrally Efficient Compatible Single-Sideband Modulation for OFDM Transmission With Direct Detection," IEEE Photon. Technol. Lett., vol. 20, pp. 670-672,

2008.

[11] W. R. Peng et al., “Experimental Demonstration of a Coherently Modulated and Directly Detected Optical OFDM System Using an RF-Tone Insertion,” OFC’08 paper OMU2.

[12] B. J. C. Schmidt et al.,” Experimental Demonstrations of Electronic Dispersion Compensation for Long-Haul Transmission Using Direct-Detection Optical OFDM,” IEEE J. Lightwave. Technol., pp. 196, 2008.

[13] D. Qian et al, ”8×11.5-Gb/s OFDM Transmission over 1000km SSMF using Conventional DFB Lasers and Direct Detection,” OFC’08, paper OMM3.

[14] A. H. Gnauck, P. J. Winzer, “Optical phase-shift-keyed transmission,” *IEEE J. Lightwave Technol.*, vol. 23, pp. 115-130, 2005.

[15] Y. Han and Guifang Li, “Theoretical sensitivity of direct-detection multilevel modulation formats for high spectral efficiency optical communications,” *IEEE J. Selected Topics in Quantum Electronics*, vol. 12, pp. 571-580, 2006.

[16] S. Walklin and J. Conradi, “Multilevel signaling for increasing the reach of 10Gbps lightwave systems,” *IEEE J. Lightwave Technol.* 17, 2235 (1999).

[17] W.R. Peng and Sien Chi, “Quantum limit of optimum four-level ASK signals with direct detection optically preamplified receivers,” Optics Express, vol. 15, pp. 2790, 2007.

[18] K. P. Ho, and J. M. Kahn, “Spectrum of externally modulated optical signals,” *IEEE J. Lightwave Technol*., vol. 22, pp.658-663, 2004.

[19] E. Ip and J. M. Kahn, “Power spectra of return-to-zero optical signals,” *IEEE J. Lightwave Technol*., vol. 24, pp.1610-1618, 2006.

[20] E. Forestieri, “Evaluating the error probability in lightwave systems with chromatic dispersion, arbitrary pulse shape and pre- and postdetection filtering,” *IEEE J. Lightwave Technol.*, vol. 18, pp. 1493–1503, 2000.

[21] G. Bosco and P. Poggiolini, “The impact of receiver imperfections on the Performance of optical direct-Detection DPSK,” *IEEE J. Lightwave Technol.*,vol. 23, pp. 842-848, 2005.

[22] C. W. Helstrom, Elements of signal detection and estimation, Prentice Hall (1995).

[23] P. J. Winzer, “Optically preamplifier receiver with low quantum limit,” *Electron. Lett*., vol. 37, pp. 582, 2001.

[24] D. J. Richardson,P. C. Teh, M. A. F. Roelens, B. C. Thomsen, C. Tian, Z. Zhang, P. Petropoulos, M. Ibsen, “Direct sequence OCDMA systems based on fibre grating technology,” ECOC2005, Paper Th2.3.6.

[25] X. Wang; N. Wada; T. Miyazaki, G. Cincotti, and K. Kitayama, “Field Trial of 3-WDM × 10-OCDMA × 10.71-Gb/s Asynchronous WDM/DPSK-OCDMA Using Hybrid E/D Without FEC and Optical Thresholding,” *IEEE J. Lightwave Technol.*, vol. 25, pp. 207-215, 2007.

[26] H. Fathallah, L. Rusch, and S. Larochelle, “Passive optical fast frequency hop CDMA communications system,” *J. Lightwave Technol.*, vol. 17, pp. 397-405, Mar. 1999.

[27] H. Fathallah and L. Rusch, “Robust optical FFH-CDMA communications:Coding in place of frequency and temperature control,” *J. Lightwave.Technol.*, vol. 17, no. 8, pp. 1284–1293, 1999.

[28] A. E. Willner et al, “Advanced Techniques to Increase the Number of Users and Bit Rate in OCDMA Networks,” *J. Selected Topic Quantum Electron.*, vol. 13, pp. 1403-1414, 2007.

[29] C. F. Lam, R. Vrijen, D. T. K. Tong, M. C. Wu, E. Yablonobitch, “Experimental demonstration of spectrally encoded optical CDMA systems using Mach-Zehnder encoder chains,” CLEO1998, Paper CThU4.

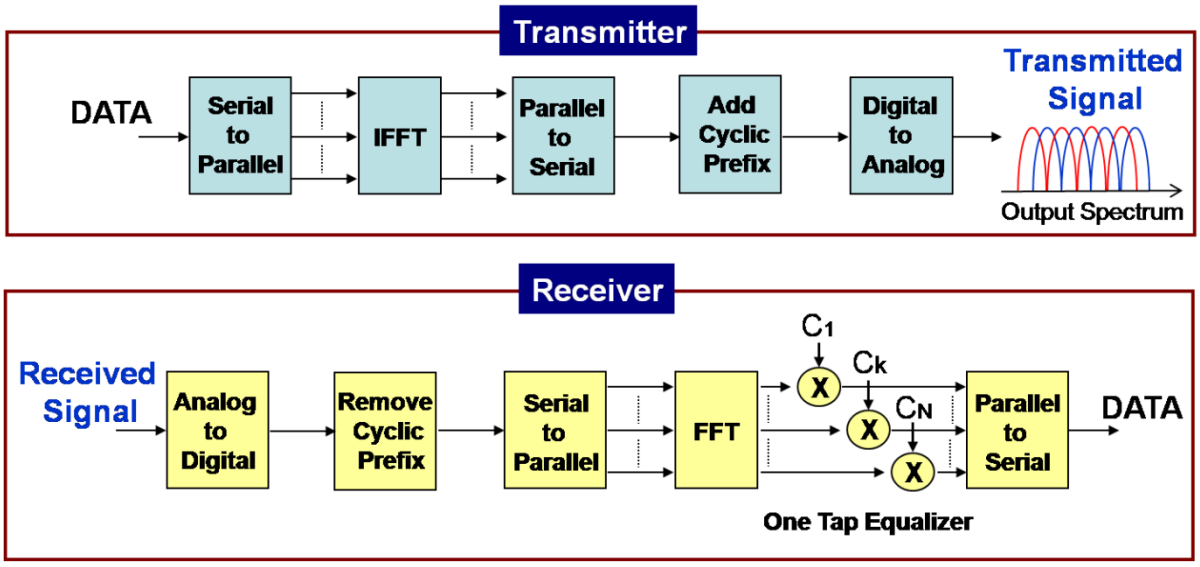

Fig. 2.1 OFDM fundamentals: transmitter and receiver.

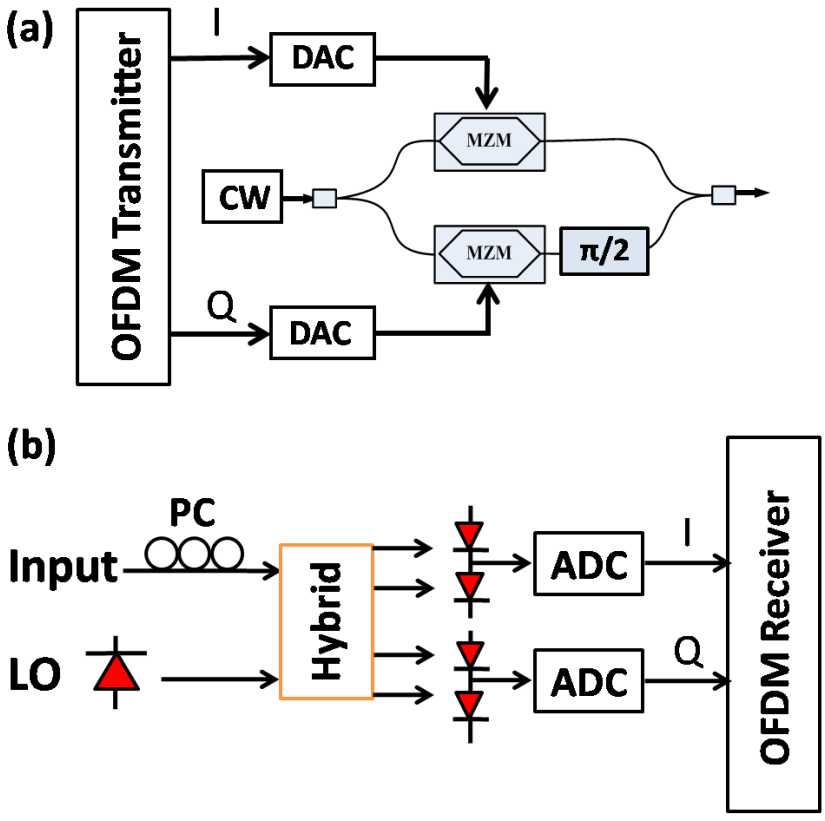

Fig. 2.2(a) The transmitter and (b) receiver in a coherent optical OFDM (CO-OFDM) system.

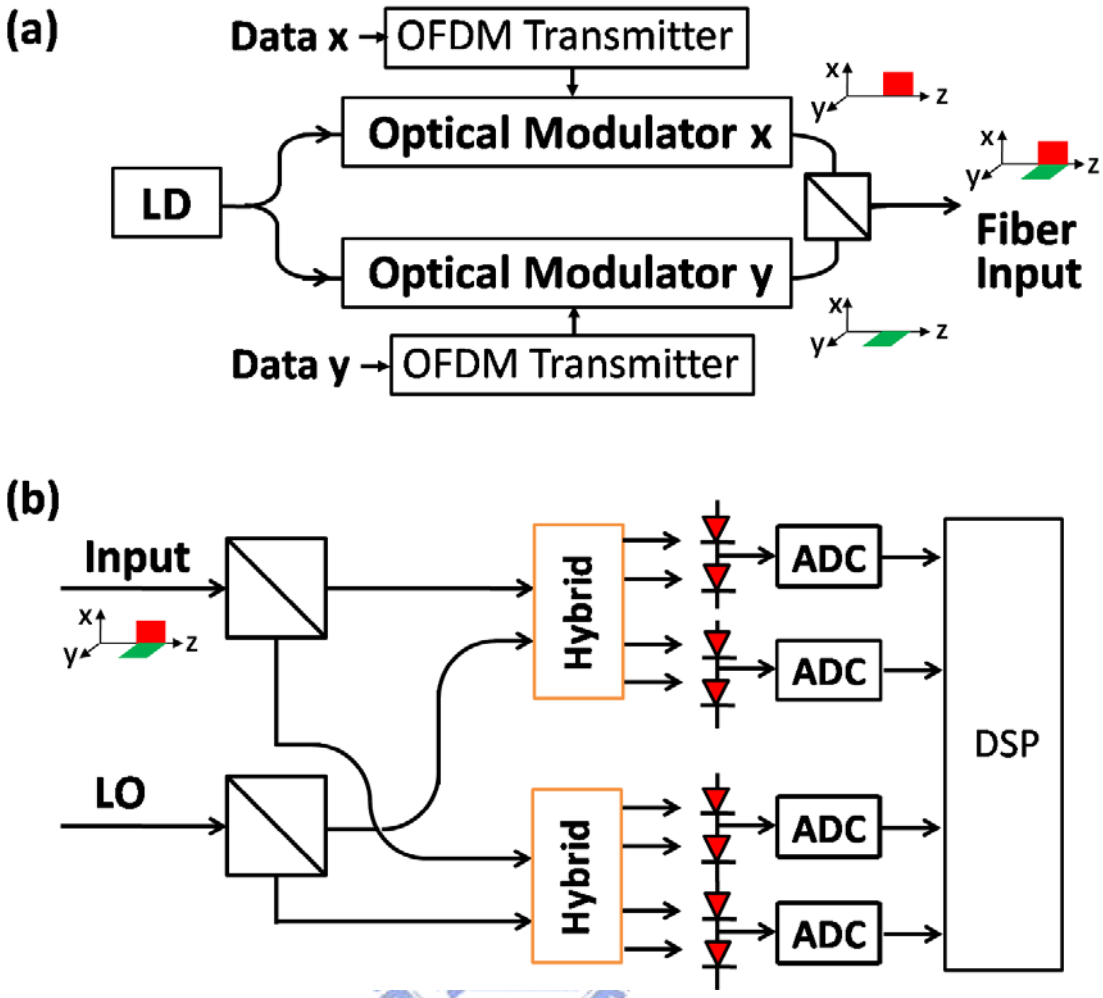

Fig. 2.3 Coherent (a) transmitter and (b) receiver for a polarization division multiplexing (PDM) OFDM system.

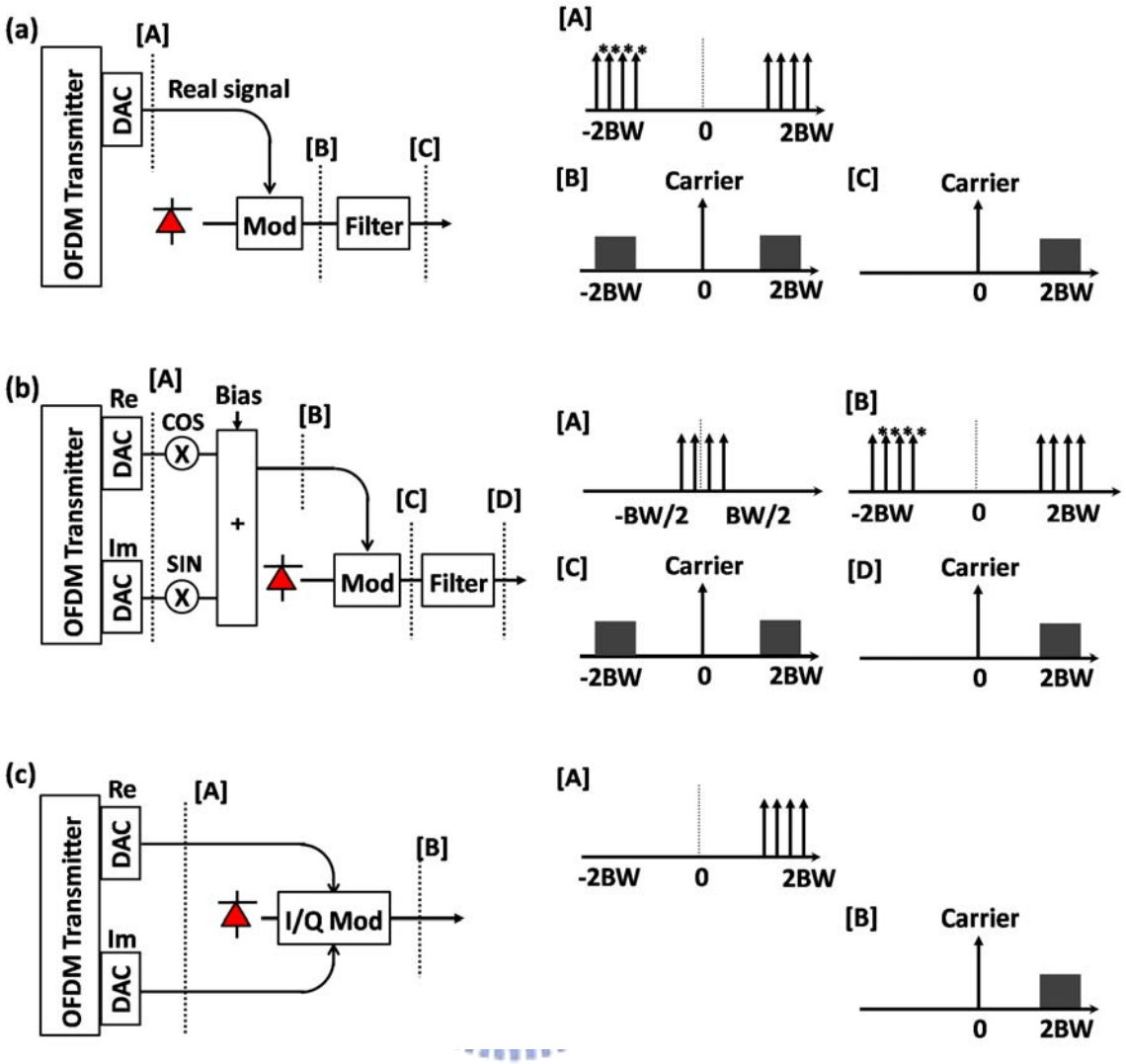

Fig. 2.4 Various proposed direct detection OFDM: (a) using Hermitian symmetry and an optical filter; (b) using upconversion and an optical filter, (c) using a frequency domain Hilbert transform. For all the three types of OFDM formats, only one photodiode is needed at the receiver.

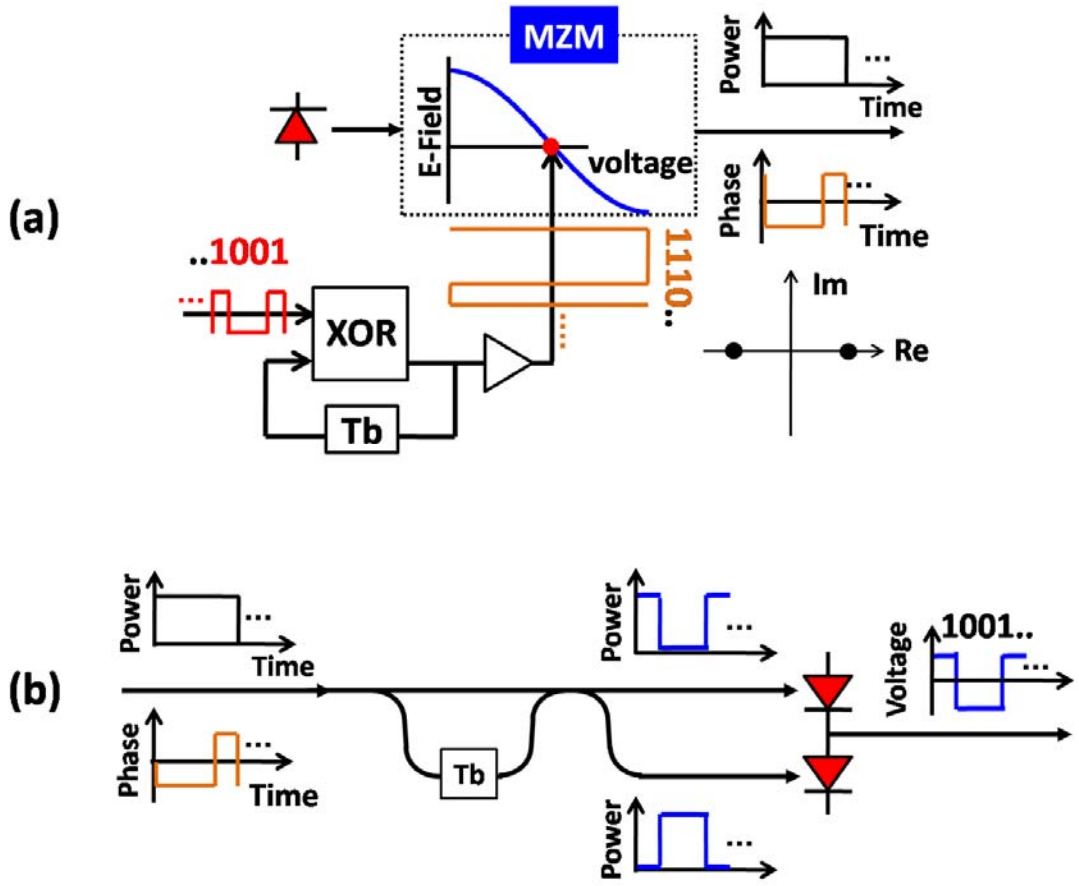

Fig. 2.5 Optical DPSK: (a) transmitter and (b) receiver.

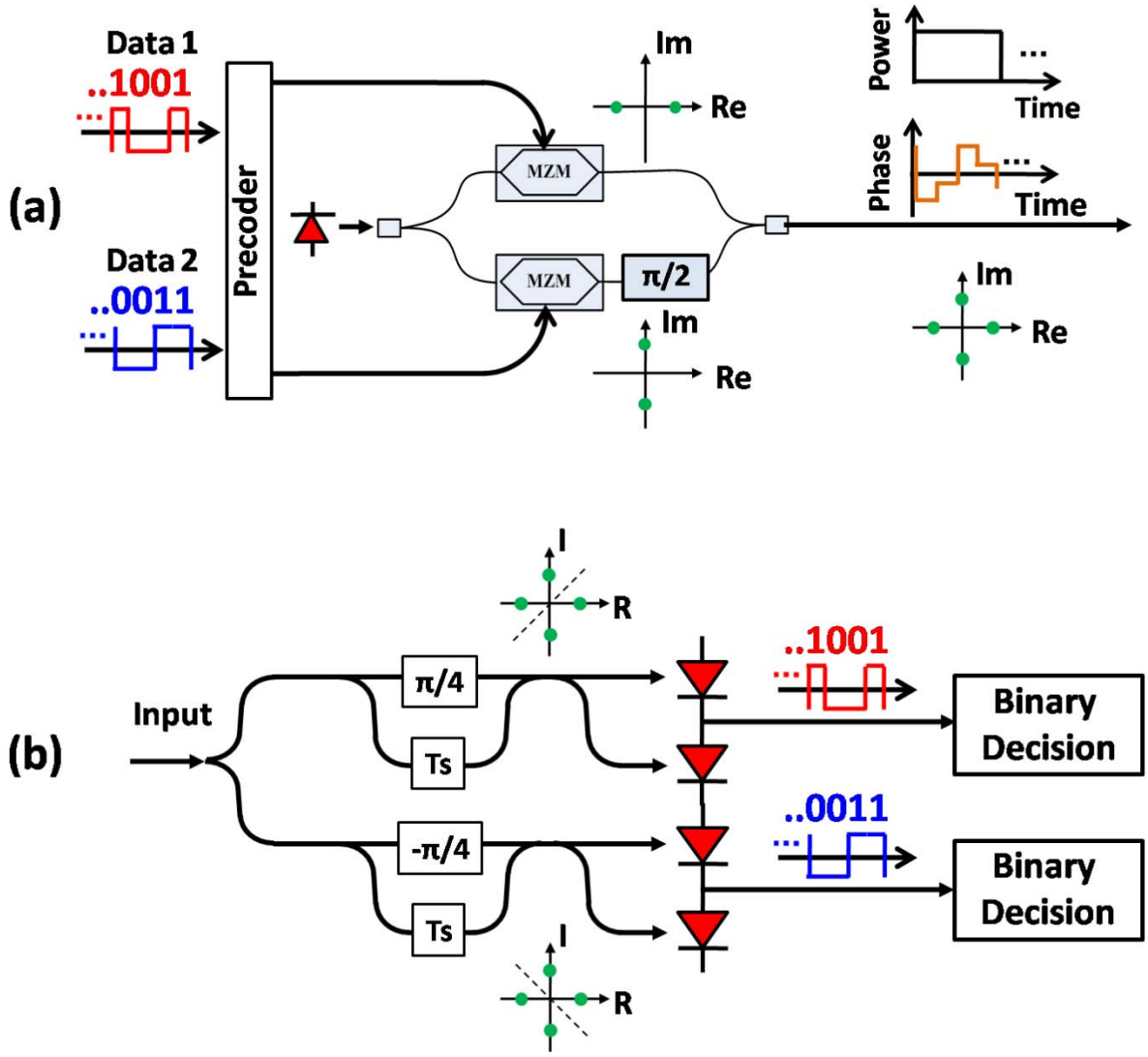

Fig. 2.6 Optical DQPSK: (a) transmitter and (b) receiver. The purpose of the two sets of optical delay interferometers is to feed the data into a simple binary decision circuit.

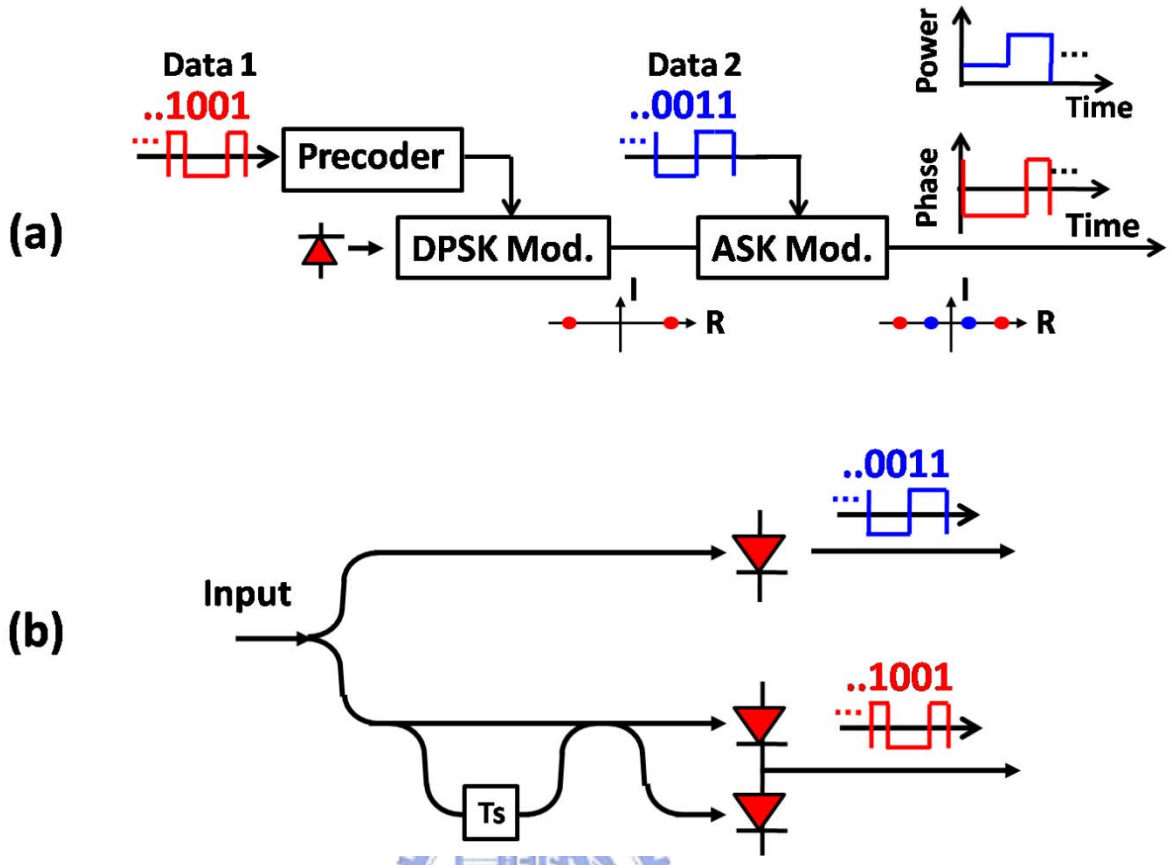

Fig. 2.7 Optical ASK/DPSK: (a) transmitter and (b) receiver.

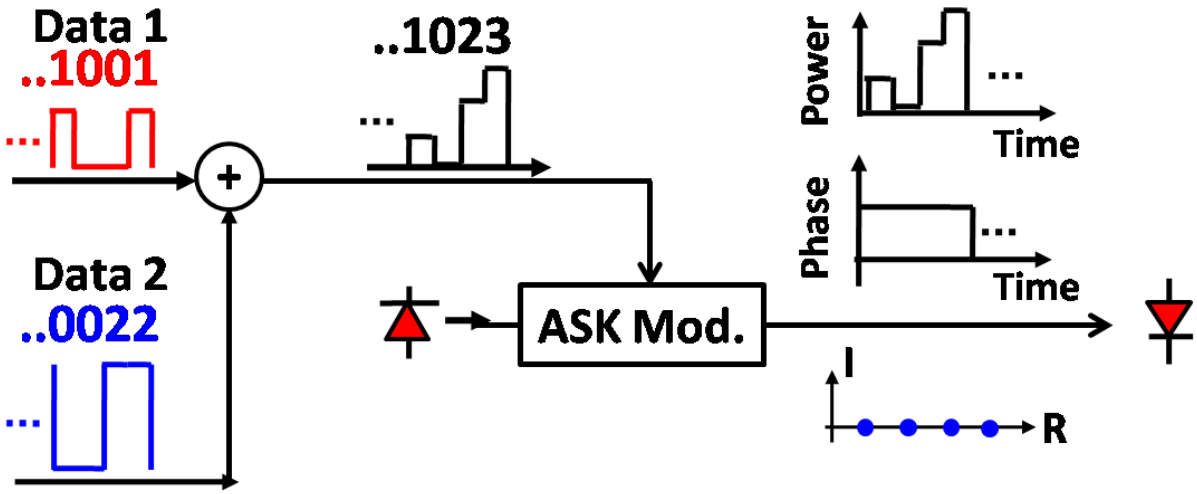

Fig. 2.8 Optical Four Level ASK (4ASK): transmitter and receiver.

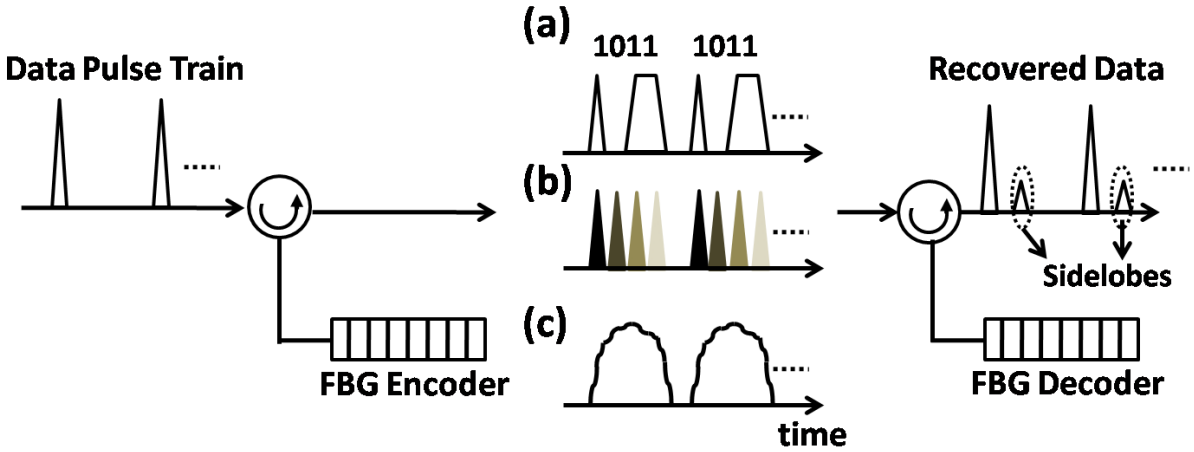

Fig. 2.9 Optical CDMA, (a) direct sequence (DS-CDMA), (b) fast frequency hopping (FFH-CDMA), (c) spectra encoding CDMA (SE-CDMA).

Chapter 3

Optical Orthogonal Frequency Division Multiplexing

3.1 Introduction

To design a baseband OFDM long-haul transmission system we should consider the following important issues, 1: receiving sensitivity, 2: CD tolerance, 3: PMD tolerance, 4: fiber nonlinearities tolerance, 5: optical filtering tolerance, 6: spectral efficiency (SE), 7: the required bandwidth of ADC/DAC, and 8: simple hardware. Actually it would be extremely hard to design formats which simultaneously address all of the above issues, but it is possible to have some format which trades several of them with the others. In this chapter, we are going to discuss couples of our proposed direct detected optical OFDM systems of which some have a better sensitivity, a better CD tolerance, a higher SE and require a lower DAC bandwidth. In all the proposed direct detected OFDM systems the receiver requires only one photodiode and thus is very simple to implement like in the conventional OOK system.

3.2 RF tone Assisted Optical OFDM Systems

In this subsection, we will introduce several our proposed techniques including **1**: the RF-tone assisted OFDM which places an RF tone at the edge of signal band for helping transfer both the optical amplitude and phase into electrical signal. This format shows a 5-dB sensitivity gain and exhibits a more robust CD tolerance compared to the power-modulated OFDM system. **2**: The post DSP compensation for impairments from MZM's I/Q imbalances and bias deviations. Over a broad range of I/Q imbalances, our approach can simultaneously compensate for the amplitude imbalance, phase deviation, bias deviation and time misalignment between the two arms of the MZM after 800 km uncompensated SSMF

transmission. **3**: The first demonstration of wavelength conversion for 10 Gbps OFDM signal using a periodically-poled Lithium Niobate (PPLN) waveguide. This proves the possibility for OFDM signals to be employed in an all-optical wavelength routing network. We also measure the relationships between the conversion penalty (efficiency) and the various OFDM parameters like the QAM sizes and subcarrier numbers. **4**: Bit error rate (BER) calculation for OFDM signal in the presence of optical pre-amplified receiver. Using Gaussian distribution for modeling the ASE beat noise, the calculated BERs are well matched to the error counting results for a broad range of QAM sizes and different bandwidth of optical filters. This would help people design and optimize an optical OFDM transmission system.

For backgrounds and overviews of OFDM, the interested readers are referred to chapter 1 and 2.

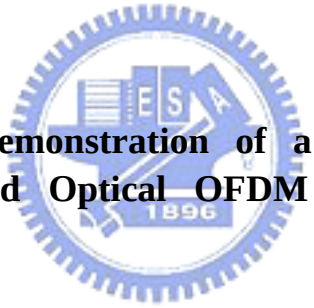

3.2.1 Experimental Demonstration of a Coherently Modulated and Directly Detected Optical OFDM System Using an RF-Tone Insertion

3.2.1.1 Introduction

Optical orthogonal-frequency-division-multiplexing (OFDM) has recently received much attention due to its potential for electrical equalization of various deleterious effects, such as chromatic dispersion (CD) [1] and polarization-mode-dispersion (PMD) [2]. In general, coherent optical OFDM exhibits better sensitivity than an incoherent system. However, the coherent approach requires a local oscillator, polarization stabilizer, and phase estimation processing at the receiver.

Alternatively, incoherent optical OFDM (IO-OFDM) combined with single-sideband transmission has been reported that uses a dual-drive Mach-Zehnder modulator (DD-MZM) [3-6]. However, that technique had a design trade-off between better sensitivity (i.e., high

modulation depth) and robustness to chromatic dispersion (i.e., from nonlinearity in the modulator) [3, 4]. In general, it would be quite advantageous to have the similar sensitivity and the transmission characteristics of a coherent system combined with the simple receiver design of an incoherent system.

In this chapter, we propose and experimentally demonstrate a coherently modulated and directly detected optical OFDM system using an inserted RF tone. We place one RF tone at the edge subcarrier for remote signal extraction after its beating with the data subcarriers. Thus, the RF tone enables coherent modulation at the transmitter and direct detection at the receiver. The optimum optical carrier to signal power ratio (CSPR) for the best sensitivity can be easily achieved by controlling the relative amplitudes of the electrical input signal. We demonstrate the RF tone assisted OFDM for an 8-QAM format at 10 Gbps. The experimental results show that the sensitivity of the proposed RF tone OFDM is 5 dB better than the conventional baseband SSB OFDM approach. After 260 km of standard single mode fiber (SSMF) transmission, there is negligible power penalty observed.

3.2.1.2 Concept

Figure 3.1(a) shows the principle of the conventional baseband SSB-OFDM [3-6]. The data and its conjugate are transferred into a time domain real-valued electrical signal by inverse fast Fourier transform (IFFT). This real-valued electrical signal and its Hilbert transform are fed into the two arms of a quadrature biased DD-MZM resulting in a SSB format. Because the signal is intensity modulated, a photodiode can transfer the optical power into photocurrent directly. To evaluate the modulation efficiency, as shown in Fig. 3.1(c), we define the optical modulation index (OMI) as $\mathrm{OMI} = (\mathrm{V_{in}})_{\mathrm{rms}}/\mathrm{V}_{\pi}$ where $(\mathrm{V_{in}})_{\mathrm{rms}}$ is the root mean square of the electrical input to the DD-MZM and V_{π} is the switching voltage of the MZM.

Figure 3.1(b) shows the proposed RF-tone assisted OFDM system with two possible subcarrier allocations. We call the two schemes OFDM-A and OFDM-B, respectively. For both allocations the RF tone for remote direct detection is placed at the leftmost subcarrier. For OFDM-A, a gap with the same width as the signal itself is used between the RF tone and the signal. For OFDM-B, odd subcarriers relative to the RF-tone are used for the data and the even subcarriers are left unused. For both schemes, the electrical OFDM signal after the IFFT is complex and its real and imaginary parts are fed into the two arms of an optical I/Q modulator. The RF-tone induced optical carrier of the proposed schemes is with a distance of B/2 away from the lightwave frequency. Due to the coherent nature of the signals, the signal-signal beat interference (SSBI) is generated after a square-law photodiode. For OFDM-A the SSBI will fall on the subcarriers within the gap and for OFDM-B the SSBI will fall on those subcarriers interleaved with the data subcarriers. Thus the data of the two allocations can be extracted without interfered by the SSBI, which makes our coherently modulated and direct detection scheme possible.

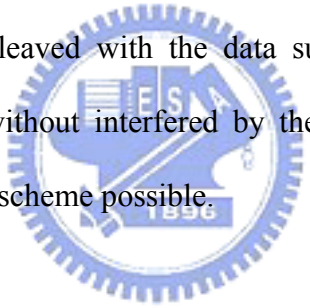

3.2.1.3 Equalization

3.2.1.3.1 Training Sequence

For OFDM we send the training sequence at the start of each transmitted OFDM packet. These data are known at the receiver and thus the channel response over each subcarriers can be approximated by comparing the received and the known data symbols.

3.2.1.3.2 One-tap Equalizer

The received electrical signal is

$$R_n = \sum \alpha^* \alpha_k A^* d_k e^{j2\pi \frac{kn}{N} + \theta_k - \theta_A}$$

The data R_k on each subcarrier k is the fast Fourier transform of the received signalR_n,

$$R_k = FFT(R_n) = \alpha^* \alpha_k A^* d_k e^{j(\theta_k - \theta_A)}$$

The channel response for each subcarrier can be approximated by comparing the received training symbols and the known symbols at the receiver.

$$H_k = R_k / d_k = \alpha^* \alpha_k A^* e^{j(\theta_k - \theta_A)}$$

Then the received signal following the training sequence is equalized by this estimated channel response:

$$\hat{d}_k = R_k / H_k$$

This very simple and general equalization method for an OFDM system is the well-known one-tap equalizer.

3.2.1.4 Experimental Setup and Results

Figure 3.2 shows the experimental setup with the proposed RF-tone assisted OFDM system. The required digital signal processing (DSP) block for the OFDM signals is emulated by Matlab program. 92 subcarriers for the data and one subcarrier for the RF tone are zero-padded with an IFFT size of 256. The data rate is 10 Gbps mapped onto a circular 8-QAM and thus the data rate of each subcarrier is 36 M symbols per second. The duration of an OFDM symbol is 27.6 ns and the cyclic prefix is 1.62 ns. The generated OFDM signal is then loaded into an arbitrary waveform generator (Tektronix, AWG7102) with a sampling rate of 10 GHz. The two outputs of the AWG, which are the real and imaginary parts of the OFDM signal, are injected into the in-phase (I) and quadrature-phase (Q) arms of an optical I/Q modulator, respectively. The output of I/Q modulator is sent into four spans of SSMF with a total distance of 260 km without any dispersion management. At the receiver, the received signal is amplified and filtered with a bandpass filter before detection by a 10 GHz photodiode. The photocurrent is then sampled at 20 GHz (Tektronix, TDS6604). The stored samples are then post-processed in Matlab for synchronization, cyclic prefix removal, FFT

and equalizations.

Figure 3.3 depicts the error vector magnitude (EVM) versus the CSPR. The EVM is shown in Fig. 3.1(d) and defined as$\text{EVM}\ [\%] = 100[\sum_{i=1}^{N} |\bar{d}_i - d_i|^2/N]^{1/2}/|d_{max}|$ where N is the number of the received symbol, d_i and $\bar{d}_i$ are the ideal and received symbols, respectively, and $d_{max}$is the maximum symbol vector in the constellation diagram. For OFDM-A and OFDM-B, the optimum CSPR is found at around 0 dB, which implies that the best sensitivity is achieved when the carrier power (RF power) equals the signal power. In Fig. 3.4 we measure the nonlinear tolerance for OFDM-A and OFDM-B by varying the input power per span. We have found that OFDM-B is better in fiber nonlinear tolerance possibly due to the larger subcarrier spacing which would suppress the four wave mixing (FWM) efficiency. In Fig. 3.5, the bit error rate (BER) performance is implemented for both the proposed system and the conventional SSB-OFDM system at 10 Gbps data rate with 8-QAM. For our system the CSPR is fixed at 0 dB and for SSB-OFDM the optimized OMI = 0.12 in its back to back (b2b) is used. The back to back sensitivities of the OFDM-A and OFDM-B are similar and both are with a 5 dB better sensitivity than the conventional SSB-OFDM. Following 260 km SSMF transmission, there are almost no penalties observed for our system. For the baseband SSB-OFDM with the b2b optimized OMI, the BER could only reach $2.34\text{x}10^{-3}$ at an OSNR = 20.2 dB.

Figure 3.6 shows the simulation results of the CD tolerance for the SSB-OFDM and the proposed RF-tone OFDM schemes. The data rate is 10 Gbps with 8-QAM. The optimized OMI for the SSB-OFDM in b2b is around 0.125, which has driven the MZM into the nonlinear region. The tradeoff between the sensitivity and the CD tolerance has been found in conventional SSB-OFDM. Since our system does not suffer that much from the nonlinear distortion of the MZM, the simulated result shows that the back to back sensitivity and the CD tolerance are both improved compared to the SSB-OFDM, which validates our

experimental measurements.

3.2.1.5 Summary

We experimentally demonstrate an RF-tone assisted optical OFDM transmission. Our system has a 5-dB better sensitivity compared to the conventional baseband SSB-OFDM system and exhibits a negligible penalty transmission after 260 km of SSMF.

3.2.2 Experimental Demonstration of Compensating the I/Q Imbalance and Bias Deviation of the Mach-Zehnder Modulator for an RF Tone Assisted Optical OFDM System

3.2.2.1 Introduction

Optical orthogonal-frequency-division-multiplexing (OFDM) is a promising modulation format for long haul transmission due to its robustness to fiber chromatic dispersion (CD) and polarization-mode-dispersion (PMD) [7, 8]. The direct detection OFDM requires only one photodiode at the receiver and thus is easy and cost-effective to install and implement [7-10]. The recently proposed interleaved RF-tone-assisted direct-detection OFDM (OFDM-B in [10]) is one of the promising formats due to its better sensitivity and robustness to the CD compared to the conventional power-modulated OFDM system [10].

Similar to other optical systems, the OFDM performance critically depends on the proper operation of the Mach-Zehnder modulator (MZM). Any I/Q imbalance, which includes the amplitude imbalance, phase deviation between I/Q arms, bias deviations and time misalignment between the I/Q arms, will degrade the channel performance. Thus, careful control and precise monitoring circuit for the MZM is required. However, it is possible to relax the requirements for the transmitter's MZM monitoring and control circuit if the impact of I/Q imbalance can be compensated by receiver-side digital signal processing (DSP).

There exists many receiver-side I/Q imbalance equalization schemes in wireless

communication [11]. Unfortunately, these techniques tend to be difficult to use on direct detection optical OFDM due to the square-law nature of the photodiode. Therefore, a laudable goal for direct-detection optical OFDM would be to compensate for both I/Q imbalance and linear channel impairments.

In this paper, we experimentally demonstrate a receiver-side compensation technique for an interleaved RF-tone-assisted direct-detection OFDM system [10]. The received data is equalized by a 2x2 matrix which can effectively cancel out the MZM imbalance effects. We test the performance of an 8-QAM, 10-Gbps signal by deliberately adding amplitude imbalance, phase deviation, bias deviation, and time misalignment. The proposed method demonstrates good performance over a wide range of I/Q imbalance and bias deviation. After 800 km of uncompensated standard single mode fiber (SSMF) transmission, the proposed method can jointly compensate the added MZM imbalance and the fiber CD, and outperforms the previous one-tap equalization method by 4 dB.

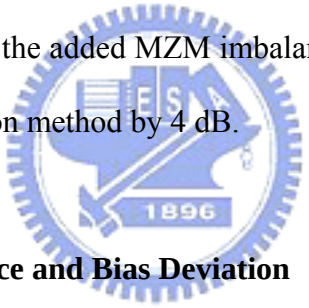

3.2.2.2 Effects of I/Q Imbalance and Bias Deviation

The MZM imbalance and compensation concept is illustrated in Fig. 3.7. Fig. 3.7(a) shows the general MZM imbalances, which includes the amplitude unbalance, phase deviation, bias deviation, and time misalignment. The MZM I/Q imbalance induces a mirrored RF tone B and a mirrored interference [11] which correlates the positive and negative sub-carriers. On the other hand, the bias deviation induces a tone C at DC since some power of the optical carrier passes through directly. The induced tones B and C result in interference after the photodiode. These interferences, as shown in Fig. 3.7(b), are: (i) mirrored interference between positive and negative sub-carriers, (ii) interference beating with tone B, and (iii) interference beating with tone C.

3.2.2.3 Compensation for I/Q Imbalance and Bias Deviation

The beating with tone C interference of (iii) can be removed by assigning the data on sub-carriers with an even spacing away from tone C (DC sub-carrier), as shown in Fig. 3.7(a). For the mirrored interference between the positive and negative sub-carriers and the beating with tone B interference, the received signal y(k) and y*(-k) is represented as a linear function of the transmitted data d(k) and d*(-k) as written in the bottom of Fig. 3.7(b). The 2x2 matrix **H** containing the channel and the imbalance information can be approximated at the receiver by using training sequences to derive the inverse matrix which is used to equalize the received data.

3.2.2.4 Experimental Setup and Results

The experimental setup is shown in Fig. 3.8. The transmitted data consists of 92 subcarriers for the data and one inserted RF tone are zero-padded with an IFFT size of 256. The data rate is 10 Gbps and the format is 8-QAM. The duration of an OFDM symbol is 27.6 ns and the cyclic prefix is 1.62 ns. The generated OFDM signal is then loaded into a 10-Gsam/s arbitrary waveform generator. The optical output of I/Q modulator is sent into the re-circulating loop containing two EDFA, a span of 80 km SSMF, and a 0.6-nm optical band-pass filter. No DCF is used during experiment. An optical pre-amplifier is used before the photodiode. The received signal is sampled and stored by a 20-Gsam/s real time scope. The demodulation, equalization and synchronization of the received OFDM signal are post-processed using Matlab digital signal processing (DSP) algorithms.

Shown in Fig. 3.9 are the measured electrical spectra of the received signal with MZM imbalances of amplitude imbalance of $\alpha = 1.38$, phase deviation of $\theta_d = 0.1\pi$, bias deviation and the time misalignment of $T_d = 10$ ps. All imbalance parameters shown in Fig. 3.10 are defined in Fig. 3.7(a).

Figure 3.10 depicts the performance in terms of error vector magnitude (EVM) versus the amplitude imbalance, phase deviation, bias deviation, and time misalignment for without and with the proposed I/Q compensation scheme. The EVM is a measure of the signal quality and a lower EVM typically means a better performance. Its rigorous definition is given in [9, 10]. All imbalance parameters shown in Fig. 3.10 are defined in Fig. 3.7(a). Our method shows a very robust tolerance to a broad range of all the imbalance effects.

We have shown that the proposed 2x2 matrix approach can effectively remove the MZM imbalance effects and provided an outstanding performance even the MZM has some imperfect operations in the case of back to back. The Fig. 3.11 depicts the BER performance before and after 800 km uncompensated SSMF transmission. This shows the proposed 2x2 matrix approach can also compensate the accumulated CD effect and has a ~2.5 dB transmission penalty after 800 km transmission. The results of the conventional one-tap equalizer are also shown in the figure. There is no extra equalization loss observed with our proposed 2x2 matrix approach. To further verify if this proposed scheme could simultaneously compensate the CD and MZM imbalance effects, we measure the required optical signal to noise ratio (OSNR) at a BER of 10^{-3} as a function of the transmission distance with the imbalance parameters shown at the left-up corner of Fig. 3.12. For back to back the signal with I/Q compensation has ~2 dB improvement over the signal without I/Q compensation. After 800 km uncompensated SSMF transmission, the transmission penalties for signal with and without I/Q compensation are ~3 and 5 dB, respectively, which means the impacts of the MZM imbalance is further enhanced after transmission. Our approach shows ~4dB gain after 800 km transmission in the presence of the added MZM imbalance.

3.2.2.5 Summary

We demonstrate an equalization technique to compensate for impairments induced by dispersion as well as I/Q imbalance and bias deviation resulted from the MZM. The proposed

scheme has a 2 dB improvement in back to back and a 4 dB gain after 800 km SSMF transmission with the MZM I/Q imbalance.

3.2.3 Tunable Optical Wavelength Conversion of a 10 Gb/s OFDM Data Signal using a Periodically-Poled Lithium Niobate Waveguide

3.2.3.1 Introduction

Optical orthogonal-frequency-division-multiplexing (OFDM) has generated much interest in our community due to the potential for robustness to various channel degrading effects as well as efficient use of the spectrum. These advantages result from using powerful post-processing techniques after the receiver and enabling long distance, uncompensated transmission systems [12, 13]. In a WDM network, the OFDM data channel can transparently traverse many wavelength-selective elements in order to avoid inefficient optical-to-electronic conversions. One impediment to fully utilizing transparency is the ability to rapidly resolve output-port contention.

As has been well documented, optical wavelength conversion of a data channel can effectively resolve contention and dramatically increase network throughput. Optical wavelength conversion has been published for most types of data modulation formats and using many types of wavelength conversion techniques [14, 15]. A key goal in any future WDM network is for the conversion approach to enable data format transparency, as well as to be broadband, high-speed, low chirp, low additive noise, efficient, and high data extinction ratio.

One method for wavelength conversion that has shown many of these characteristics is the periodically-poled lithium-niobate (PPLN) waveguide [16], which has been used to convert baseband data that was encoded in amplitude and phase. However, we are not aware of any wavelength conversion of OFDM data channels.

In this paper, we experimentally demonstrate tunable optical wavelength conversion over 30 nm with < 3 dB penalty of a 10-Gb/s OFDM signal using a PPLN waveguide. BER measurements are performed after wavelength conversion with different QAM sizes and subcarrier numbers.

3.2.3.2 Concept

Shown in Fig. 3.13 is a conceptual block diagram of tunable wavelength conversion using a PPLN waveguide in a 2-pump configuration. An input signal (f_{signal}) is converted to $f_{converted}$ through sum-frequency-generation followed by difference-frequency-generation (SFG/DFG). The output wavelength of the PPLN waveguide is tunable through the choice of the dummy signal (f_{dummy}).

Fig. 3.14 shows the experimental setup. The interleaved RF-tone assisted 10 Gb/s OFDM signal is generated by Matlab program offline [17, 18] and then loaded into the 10 GS/s arbitrary waveform generator. The inserted RF tone and 92 data subcarriers are zero-padded to an IFFT size of 256. A cyclic prefix of 1/16 of the symbol duration is applied for the margin of synchronization offsets and the inter-symbol interference. The modulated optical OFDM signal, combined with the pump and dummy, is sent to an EDFA before sent into the PPLN. The converted signal is filtered out by a 0.25 nm band pass filter (BPF) and then sent to a variable optical attenuator to adjust the received OSNR, followed by an EDFA and a 0.25 nm BPF before detection. The electrical signal is then sampled at 20 GS/s by a real time scope and post-processed in Matlab offline for synchronization, cyclic prefix removal, FFT and equalizations.

3.2.3.3 Experimental Results

Shown in Fig. 3.15 are the optical spectra after the PPLN at several converted

wavelength locations. The PPLN waveguide is temperature controlled to have a quasi-phase matching (QPM) location of ~1553 nm. The conversion efficiency over ~30 nm bandwidth is ~ -5 dB, relative to the input signal power to the PPLN. Note that the converted wavelength cannot be generated at the QPM and the pump wavelength. The gaps can be avoided through temperature tuning of QPM wavelength [16]. Fig. 3.15 (d) shows the spectra of the input and converted OFDM signal. We observe that the carrier to signal power ratio (CSPR) is preserved after the wavelength conversion.

To assess the performance of the wavelength converter, we measured the bit error rate (BER) versus OSNR/0.1 nm both back-to-back and after conversion at several locations. Shown in Fig. 3.16 are the BER curves and the corresponding constellations. Approximately 1 dB penalty at 10^{-3} BER is observed at 1538.5 nm and 1565 nm. For the converted signals that are close to the QPM, i.e. 1554.4 nm, we observe an ~3 dB penalty, which could be attributed to the relatively larger nonlinearity as the converted signal approaches to the QPM.

QAM size is also varied to evaluate the performance of the wavelength converter. Fig. 3.17 compares the BER performance of 8-QAM and 16-QAM for both the back to back case and the conversion to 1565 nm. The penalty is increased by about 1 dB when the QAM size is increased from 8 to 16. The reason could be that OFDM signal with a larger QAM size is more vulnerable to the nonlinear distortion induced during the wavelength conversion. The corresponding constellations are inserted in the figure.

Furthermore, we change the subcarrier numbers with a fixed QAM size (8-QAM). The BER versus OSNR/0.1 nm is shown in Fig. 3.18 for both back to back and the converted signal at 1565 nm. We observe that the penalty almost keeps the same as we increase the subcarrier numbers, which shows the performance of our wavelength converter is not dependent on the subcarrier numbers.

3.2.3.4 Summary

We experimentally demonstrate tunable wavelength conversion of 10 Gb/s RF-tone assisted OFDM signal with high conversion efficiency over ~30 nm tuning range using a PPLN waveguide. A penalty of < 3 dB is obtained after wavelength conversion with different QAM sizes and subcarrier numbers.

3.2.4 Theoretical Investigations

3.2.4.1 The Optimum Carrier to Signal Power Ratio (CSPR)

Based On previous numerical results, there is an optimum power ratio between the carrier and signal. Differing from the previous method, we derive the electrical signal power in terms of the received optical power and the carrier to signal power ratio (CSPR). The optimum value of 0 dB is found and it is the same as the previous numerical method, thus validating our derivation.

The optical field signal can be written as:

$$S_n = \frac{1}{\sqrt{N}}[A + \sum_{k=0}^{N-1} d_k exp\,(\frac{j2\pi f(k)n}{N})]$$

The averaged optical power,

$$P_{opt} = E[|S_n|^2] \propto E\left[\left|A + \sum_{k=0}^{L-1} d_k\, exp\left(\frac{j2\pi f(k)n}{N}\right)\right|^2\right] =$$

$$E[|A|^2] + E\left[\left|\sum_{\substack{k=0 \\ k\neq\frac{N}{2}+1}}^{N-1} d_k\, exp\left(\frac{j2\pi kn}{N}\right)\right|^2\right] = E[|A|^2] + E[\sum_{k=0}^{L-1}|d_k|^2] =$$

$$|A|^2 + E[\sum_{k=0}^{L-1}|d_k|^2].$$

The useful signal current from beating between the RF tone and the signal is expressed as

$$I_{sig} = 2Re[A\,(\sum_{k=0}^{L-1} d_k ex\,p\left(\frac{j2\pi f(k)n}{N}\right))^*] .$$

The electrical signal power could be written as $P_{el} = E[I_{sig}I_{sig}^*] = E\left\{4 \times \left(R_e\left[A \times \sum_{k=0}^{L-1} d_k^* exp\left(\frac{-j2\pi f(k)n}{N}\right)\right]\right)^2\right\} = E\left\{4 \times A^2\left[\sum_{k=0}^{L-1}|d_k|\cos\left(\frac{2\pi\left(\frac{N}{2}+1-f(k)\right)n}{N} - \theta_{d_k}\right)\right]^2\right\} =$

$2\,A^2\,E[\sum_{k=0}^{L-1}|d_k|^2] \le 1/2 * (A^2 + E[\sum_{k=0}^{L-1}|d_k|^2])^2$

The equality for optimum receiving holds when

$A^2 = E[\sum_{k=0}^{L-1}|d_k|^2]$

Thus the CSPR for optimum receiving is

$$CSPR = A^2/E[\sum_{k=0}^{L-1}|d_k|^2] = 1\ (0\ dB)$$

$$P_{el} = P_{OPT}\text{^}2/2$$

where P is the optical received power. So the optimum CSPR is located at 0 dB, which matches the previous numerical results. Note that a factor "2" in the denominator and the half power of the inserted RF tone contribute a 6 dB worse sensitivity than a coherent system.

3.2.4.2 Bit Error Rate Calculation for a Single Sideband OFDM Signal with Direct Detection optically Pre-amplified Receivers

3.2.4.2.1 Introduction

Optical orthogonal-frequency-division-multiplexing (OFDM) has recently been proposed as a promising format for optical long haul applications. Many reports have focused on its performance evaluation under the optical filtering, CD and PMD effects [19, 20]. So far, the best figure of merit for OFDM performance evaluation is the bit error rate (BER) obtained by error counting method. However, that method is typically time and memory consuming because lots of OFDM blocks should be generated and then counting errors bit by bit. Thus, an accurate and high efficient BER calculation is crucially required for optimizing an OFDM system.

Recently, a Q-factor approach which uses the averaged signal to noise ratio (SNR) of all subcarriers and Gaussian assumption for the noise distribution is suggested approximating the BER of a 4-QAM SSB-OFDM format [19]. However, there is no evidence in [19] to evaluate how well this Q-factor approach can match the practical error-counting method in an OFDM system. In general, the Thus, the appropriateness of the Q-factor approach extracted from the constellation points, which has not considered the individual signal to noise ratio (SNR) of each subcarrier, and the suitability of the Gaussian assumption to the received electrical beat noises are still unsolved yet.

In this paper, we show that the exact BER of a SSB-OFDM signal can be accurately approximated by estimating the SNR of each subcarrier separately and averaging the BERs of all subcarriers. The SNR of each subcarrier is derived by numerically computing the power spectral density (PSD) of the signal and the electrical beat noises. We have found that the beat noise is colored and the subcarriers are with different powers due to the filtering effect, thus yielding a non-uniform SNR distribution over all subcarriers. The numerical results, supported by the error counting method, show our scheme can well predict the exact BER even under a tight optical filtering. Moreover, although a larger QAM size is more spectrally efficient, the OSNR penalties at a BER of 10^{-9} for the 16- and 64-QAM are 3.82 and 8.19 dB, respectively, relative to the 4-QAM format by using our proposed BER evaluation approach.

3.2.4.2.2 Subcarrier Signal to Noise Ratio and Bit Error Rate

Figure 3.19 shows the receiver model for an optical SSB-OFDM signal in the presence of optical pre-amplifier. The signal along with the white accumulated spontaneous emission (ASE) noise passes through an optical filter to remove the residual ASE noise and enters a photodiode for direct detection. The spectra of the signal and the ASE after the filter are shown in the insets of Fig. 3.19. As the squared-law nature of a photodiode, we can write the photocurrent as $I = |S + N|^2 = |S|^2 + 2\mathrm{Re}(SN^*) + |N|^2$ where S is the optical OFDM

signal including the carrier and N is the ASE noise. The first term, $|S|^2$, contains the DC current, carrier-signal beat signal (signal) and signal-signal beat interference (SSBI). The second term, $2\mathrm{Re}(SN^*)$, is the signal-ASE beat noise (SABN) and with a PSD denoted as $N_{SA}(f) = N_s(f) * N_A(f) + N_s(-f) * N_A(-f)$ where N_s and N_A are the baseband PSD of the optical signal and the ASE, respectively, and $*$ is the convolution operator. This implies that the SABN is colored if ASE is band-limited by an optical filter. The third term $|N|^2$ is the ASE-ASE beat noise (AABN) and with a PSD of $N_{AA}(f) = N_A(f) * N_A(f) + N_{AA}(0)$. Again the band-limited ASE will yield a colored AABN although its effect is insignificant due to its relatively low power. Assuming that the SABN and AABN are independent, the total noise PSD will be $N_{SA}(f) + N_{AA}(f)$. To evaluate the signal power of each subcarrier, we use one OFDM block with the predetermined optical power passing through the optical filter with the consideration of the filtering effect over the subcarriers, and then we can get the electrical signal power after converting this optical block into electrical domain. We define the $SNR_i = E_i/N_i$ as a power ratio of the signal to the noise for the i-th subcarrier. Assuming the beat noise is Gaussian distributed, we can relate the SNR_i to the BER_i of each subcarrier as $BER_i = (1 - 1/L)/\log_2 L \times \mathrm{erfc}(\sqrt{3SNR_i \log_2 L/[(L^2 - 1)\log_2 M]})$, where L is the number of levels in each dimension of the M-ary modulation system for each subcarrier [21]. Then the ensemble BER will be the mean of the error rate of each subcarrier, $BER = \langle BER_i \rangle$.

3.2.4.2.3 Results and Discussions

Figure 3.20 depicts the PSD of the signal and the beat noises with an OSNR of 16 dB. The simulated data rate is 10 Gbps with a 4-QAM format. The optical carrier to signal power ratio is set at the optimum of 0 dB [19]. The signal bandwidth Bs is ~11.6 GHz after the insertion of the cyclic prefix, which occupies 1/16 duration of one OFDM block and filtered by a 2nd order Gaussian type optical filter with a 3-dB bandwidth of 12 GHz. The PSD of the signal,

SABN and AABN are not constant and thus each subcarrier will have a different SNR. In Fig. 3.21 we evaluate the system BER versus the optical signal to noise ratio (OSNR) with our method under three different optical bandwidths: 8, 13 and 20 GHz. Zero forcing equalization is used for its simplicity in this paper [20].The BER by error counting is also shown to validate our numerical results. Under different optical bandwidths, our method still keeps a good approximation for a tight optical filtering (OWB = 8 G) while the Q-factor estimation of all the constellation points [19] fails to predict the exact BER. In Fig. 3.22, we extend the QAM size from M = 4 to 16 and 64 and find their receiving sensitivities under their optimum optical bandwidth of 13, 6.7 and 4.6 GHz, respectively. The numbers of the data subcarrier are 72, 36, and 24, respectively, for M = 4-, 16-and 64-QAM and all are zero-padded with an IFFT size of 512. The error counting method indicates that our method still work for a larger constellation size. Additional 3.82 and 8.19 dB signal power are required if we extend the QAM size to M = 16 and 64 to reach a higher spectral efficiency. Note that these results are simulated under the assumption of equal transmission power among the subcarriers. Adaptive power control for each subcarrier would yield a better performance.

3.2.4.2.4 Summary

We provide a fast and accurate BER calculation for a SSB-OFDM signal by considering the SNR of each individual subcarrier. The numerical results show that our scheme can accurately evaluate the BER for different QAM formats even under a strong optical filtering.

3.3 Virtual Single Sideband OFDM (VSSB-OFDM)

In this sub-section we will discuss couples of our proposed spectrally-efficient and robust CD tolerant OFDM format which we referred to as virtual single sideband OFDM (VSSB-OFDM). Like the RF tone assisted OFDM, an RF tone is placed at the edge of the signal band for remote beating. The difference between the RF-tone assisted and VSSB-OFDM is that for

RF-tone assisted OFDM the signal-signal beat interference (SSBI) is avoided by using some blank subcarriers while for VSSB-OFDM the SSBI is mitigated by using the iterative estimation and cancellation technique. Because no blank subcarriers are used in VSSB-OFDM, the spectra efficiency (SE) is higher than RF-tone assisted OFDM at a price of an extra signal processing for iterative detection. Because of its narrower bandwidth, we demonstrate the first 4-QAM and 10-Gbps direct detected field modulated OFDM signal with a direct up-conversion I/Q modulator. The 10-Gbps VSSB-OFDM signal occupies only ~5.2 GHz and thus is very spectrally efficient. Compared to the conventional power modulated OFDM, our system has a better sensitivity as well as a better CD tolerance. After 340 km standard single mode fiber transmission, there is negligible penalty observed. Then we further propose the generalized version of this format called Generalized VSSB-OFDM (GVSSB-OFDM) which trades the transmission performance with the signal bandwidth within the available DAC bandwidth. With an optimum gap between the RF tone and the signal, we successfully transmit the GVSSB-OFDM through 1600 km uncompensated SSMF with ~ 3 dB penalty.

The backgrounds and overviews are described in Chapter 1 and 2.

3.3.1 Experimental Demonstration of 340 km SSMF Transmission Using a Virtual Single Sideband OFDM Signal that Employs Carrier Suppressed and Iterative Detection Techniques

3.3.1.1 Introduction

Optical orthogonal-frequency-division-multiplexing (OFDM) is a promising technique for long-haul transmission since it provides a path for electronic equalization of chromatic dispersion (CD) and polarization-mode-dispersion (PMD) [22-23]. Within the topic of OFDM systems, incoherent optical OFDM combined with the single-sideband format (SSB-OFDM)

can overcome the power fading inherent in a double-sideband system [22].

Typically, SSB-OFDM requires a steep optical filter to simultaneously remove one of the sidebands and suppress the optical carrier power simultaneously [24]. Unfortunately, a spectrally-inefficient guard-band between the optical carrier and the data signal is typically needed to avoid inter-modulation distortion near the optical carrier. A recent report that does not need this guard-band for SSB-OFDM uses a dual-drive Mach-Zehnder modulator (DD-MZM) [25]. However, that spectrally-efficient technique has a design trade-off between better sensitivity (i.e., high modulation depth) and robustness to chromatic dispersion (i.e., from nonlinearity in the modulator) [26].

In general, a key issue is that the generation of the SSB-OFDM typically requires the electrical sampling rate to be double the transmitted optical signal bandwidth. Therefore, half the electrical bandwidth has not been used for data and is "wasted." A laudable goal would be to generate SSB-OFDM in the transmitter in which only half the electrical bandwidth is needed and yet still preserves a high sensitivity and the tolerance to chromatic dispersion.

In this paper, we propose and demonstrate a virtual SSB-OFDM (VSSB-OFDM) direct-detection technique that uses half the electrical bandwidth by employing an RF tone insertion and iterative detection. Since the optimum optical carrier to signal power ratio (CSPR) for best receiving sensitivity can be controlled from the electrical RF signal directly, there is no trade-off between the sensitivity and the CD tolerance. We successfully transmit 10 Gbps data with a 4-quadrature amplitude modulation (4-QAM) using our VSSB-OFDM signal over 340 km of standard single mode fiber (SSMF). The results show that both the back to back sensitivity and the CD tolerance are improved with this VSSB-OFDM format.

3.3.1.2 Concept

Figure 3.23(a) and (b) shows the transmitter architectures of the conventional baseband

SSB-OFDM [25, 27] and the proposed VSSB-OFDM system, respectively. For the SSB-OFDM, the data, together with their conjugates, are transferred into a real baseband signal after inverse Fast Fourier Transform (IFFT). This real-valued electrical signal and its Hilbert transform are fed into the two arms of a quadrature-biased dual-drive MZM (DD-MZM) resulting in a SSB format. We define the optical modulation index, $\mathrm{OMI} = (V_{in})_{rms}/V_{\pi}$ where $(V_{in})_{rms}$ is the root mean square of the electrical input to the DD-MZM and V_{π} is the switching voltage of the MZM, as an evaluation of the modulation efficiency.

For the proposed VSSB-OFDM, we place one RF tone for remote beating at the left-most subcarrier. This RF subcarrier together with the data subcarriers are transferred into a complex baseband signal by IFFT. Because our system does not require the redundant subcarriers for the conjugates of the data, our system saves half the electrical bandwidth compared to the conventional SSB-OFDM. The real and imaginary parts of the signal are injected into the in-phase (I) and quadrature-phase (Q) arms of an optical I/Q modulator. The original carrier is suppressed and a new carrier induced by the inserted RF tone appears at the left-most subcarrier. Note that the carrier to the signal power ratio, which is defined as $\mathrm{CSPR} = 10\log(|A|^2/\sum|d_i|^2)$ where A and d_i are the subcarrier amplitudes of the RF tone and data, can be easily optimized by controlling the electrical RF signal. Because the signal is coherently modulated in nature, the beating among the data subcarriers at the photodiode will yield a non-negligible interference called the signal-signal beat interference (SSBI) to the signal. To remove the SSBI, we introduce an iterative cancellation technique in the receiver, as shown in Fig. 3.24. The principle of this technique follows: (i) The photocurrent is firstly stored in memory and is used to made decisions. (ii) Using the decisions to reconstruct the SSBI. (iii) Subtract the rebuilt SSBI from the stored photocurrent and make decisions. (iv) Repeat (ii)-(iii) until the constellation converges.

3.3.1.3 Equalization

3.3.1.3.1 Training Sequence

Since the iteration detection would require the channel response of all the transmitted data subcarriers, the training sequence should be properly designed for preventing it being suffered from the SSBI.

The training sequence used for VSSB-OFDM system is the interleaved RF-tone OFDM described in subsection 3.2. The training data are only allocated on even subcarriers and the other odd subcarriers are left unused. After the photodiode, the training data will not suffer the SSBI and their frequency responses could be evaluated with the conventional approach. As for the frequency responses of those unused subcarriers, they could be approximated by interpolating the already known frequency responses of the even subcarriers. Thus, the frequency responses of half the subcarriers are known at the receiver for equalization. Therefore, the channel response over all subcarriers can be evaluated and can be used for SSBI removing iterations.

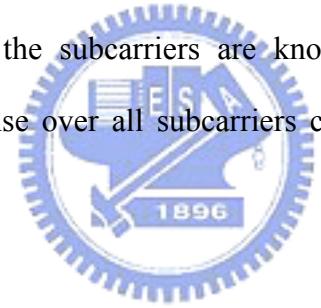

3.3.1.3.2 Iterative Estimation and Cancellation Equalization

The SSBI usually is non-ignorable over a broad range of signal CSPR. To promise an acceptable performance, the SSBI can be removed by a decision feedback iterative equalization. The transmitted optical signal can be written as: $S_n = A + \sum d_k e^{j2\pi\frac{kn}{N}}$

, the data signal after the photodiode is $I_n = 2Re[A^* \sum d_k e^{j2\pi\frac{kn}{N}}]$

$$R_n = |\alpha A|^2 + Re[\sum \alpha\alpha_k A d_k e^{j2\pi\frac{kn}{N}+\theta_k-\theta_A}] + \left|\sum \alpha_k d_k e^{j2\pi\frac{kn}{N}+\theta_k}\right|^2$$

The channel response for each subcarrier is

$$H_k = \alpha\alpha_k A e^{j(\theta_k-\theta_A)}$$

And the equalized symbol is

$$R_k^0 = FFT(R_n)/H_k$$

Where the first decisions of R_k^0 is d_k^0.

The iterative process implements the following steps:

(i) Reconstruct the interference by using d_k^i

$$I_n^i = \frac{1}{|\alpha A|^2}\left|\sum H_k d_k^i e^{j2\pi\frac{kn}{N}}\right|^2 = \left|\sum \alpha_k d_k^i e^{j(2\pi\frac{kn}{N}+\theta_k)}\right|^2$$

(ii) Subtract the interference and get the equalized symbols

$$R_k^{i+1} = FFT(R_n - I_n^i)/H_k$$

(iii) Make decisions for R_k^{i+1} and we get d_k^{i+1}

(iv) Repeat (i) to (iii) until the symbol converges

Since each iteration requires one FFT and IFFT computations, the recovering algorithms should be powerful enough to reduce the number of required iterations.

3.3.1.4 Experimental Results

Figure 3.25 depicts the configuration of the VSSB-OFDM transmitter and the receiver. The OFDM signal is firstly generated by Matlab program offline and then loaded into the 10 Gsam/sec arbitrary waveform generator (Tektronix AWG7102) which functions as a digital to analog converter (DAC). The subcarrier number for the RF tone and data is 145 and is zero-padded to an IFFT size of 256. A cyclic prefix of 1/16 of the symbol duration is applied for the margin of synchronization offsets and the inter-symbol interference (ISI). The data rate is 10 Gbps with a format of 4-QAM. An optical I/Q modulator is fed with the two outputs of the AWG, which are the real and the imaginary parts of the generated OFDM signal. The optical output of the I/Q modulator is transmitted over standard single mode fiber (SSMF) with a distance of 340 km without optical dispersion compensation. An optical preamplifier followed by an optical bandpass filter with a 3-dB bandwidth of 0.3 nm is used before a photodiode. The photocurrent is digitally sampled and recorded by a high speed real time scope (Tektronix, TDS6604) with a bandwidth and sampling rate of 6 GHz and 20 Gsam/sec,

respectively. Synchronization, FFT, equalizations and iterative cancellation are implemented offline in Matlab program. The insets show the RF spectrum and constellations for the received 4-QAM signals without and with the iterative cancellation scheme.

Figure 3.26 shows the error vector magnitude (EVM) versus the iteration number for different CSPR. The definition of EVM is $\text{EVM}\,[\%] = 100[\sum_{i=1}^{N} |\bar{d}_i - d_i|^2/N]^{1/2}/|d_{max}|$, where N is the number of symbols, $\bar{d}_i$ and d_i are the received and ideal symbols, respectively, and $d_{max}$is the maximum symbol vector in the constellation diagram. A lower CSPR (i.e., 2 dB) requires more iterations due to the relatively high power of the SSBI to the signal. For a higher CSPR (6 dB or higher), two iterations are about to converge. As a result, we choose 4 as the iteration number for the following measurement, which is more than required. The measured EVM as a function of the CSPR is shown in Fig. 3.27. The CSPR of 4 dB is found optimum for the system, which implies the best receiving sensitivity. The bit error rate (BER) performance shown in Fig. 3.28 is implemented based on error counting method for both the conventional SSB-OFDM and VSSB-OFDM. Due to the high requirement for the electrical bandwidth (i.e., the sampling rate of the AWG) of the conventional SSB-OFDM, the minimum constellation size limited by the 10-G AWG for 10 Gbps data will be 8-QAM. The required OSNR at a BER of 10^{-3} for our system is 5 dB better than the conventional SSB-OFDM, which has been optimized with OMI = 0.12 in back to back. The 5-dB gain is attributed to the optimum CSPR (the better sensitivity of VSSB-OFDM will be shown in Fig. 3.29) and the smaller constellation size used in VSSB-OFDM. Following 340 km SSMF transmission, there is negligible penalty observed for our system. The conventional SSB-OFDM signal, which suffers from the nonlinearity of the MZM, could only reach a BER of $2.34\text{x}10^{-3}$ at an OSNR = 20.2 dB after 260 km transmission.

The simulation comparisons for the CD tolerance between the conventional SSB-OFDM and VSSB-OFDM are depicted in Fig. 3.29. The data rate and format for the SSB-OFDM and VSSB-OFDM are 10 Gbps and 4-QAM. For the conventional SSB-OFDM, clipping the input

electrical signal which prevents overshoot has been employed for a better sensitivity [28]. The optimum OMI for the SSB-OFDM is found at ~0.125, which is limited by the nonlinearity of the MZM. The results show that VSSB-OFDM is at least with a 2-dB better sensitivity and a more robust CD tolerance.

3.3.1.5 Summary

We have demonstrated a virtual SSB-OFDM system which put an RF tone at the edge of the signal band for remote beating. The signal has a ~5 dB better sensitivity and a more robust CD tolerance compared to the conventional power modulated OFDM.

3.3.2 Generalized Virtual SSB-OFDM (GVSSB-OFDM)

3.3.2.1 Introduction

Optical orthogonal-frequency-division-multiplexing (OFDM) has attracted great attention due to the ability of receiver-side electronic signal processing to compensate for various channel impairments, including fiber chromatic dispersion (CD) and polarization-mode-dispersion (PMD) [29-30]. Within the topic of optical OFDM, direct detection combined with single-side band (SSB) format shows good tolerance to CD and yet only requires a single photodiode in the receiver [29-32].

A promising alternative format is virtual-single-side band OFDM (VSSB-OFDM) [31]. In this approach, the original optical carrier is suppressed and an additional RF tone is inserted in order to induce remote beating. When compared to other direct up-converted transmitters, this format is spectrally efficient in the electronic domain, is tolerant to CD, and relaxes the electrical bandwidth requirement for digital-to-analog converters (DAC) [29, 31]. The performance trade-off for the VSSB-OFDM is the increased signal-signal beat interference (SSBI), which is typically higher in-band near the RF tone and requires multiple iterations for removal [31]. Moreover, the extreme distortion after a long haul transmission

would destroy the SSBI reconstruction efficiency, thereby making data recovery quite difficult.

For VSSB-OFDM systems, the in-band SSBI can be reduced if we put a frequency gap between the RF tone and the signal. However, a large frequency gap would produce increased out-of-band image interference even if pre-emphasis is used [33]. Therefore, a trade off between the SSBI and the image interference exists. A laudable goal would be to judiciously determine the frequency gap to optimize the system performance.

In this paper, we experimentally demonstrate a generalized VSSB (GVSSB)-OFDM technique that provides an optimized frequency gap between the inserted RF tone and the signal, thereby trading SSBI with the image interference. This format shows less sensitivity to any variations in the carrier-to-signal-power ratio (CSPR). It also requires fewer post-processing iterations for interference cancellation. This method has ~3 dB optical signal-to-noise ratio (OSNR) penalty after 1600 km standard single mode fiber (SSMF) without optical dispersion compensation, while the previous regular VSSB-OFDM without the gap has a ~10 dB penalty.

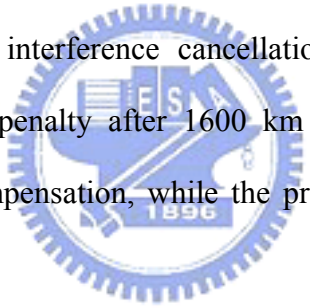

3.3.2.2 Concept

Figure 3.30 shows the GVSSB-OFDM format with a tuneable gap. Within the available sampling rate of the DAC, a larger gap would suffer a smaller SSBI but a larger image interference while a smaller gap would suffer a larger SSBI but a smaller image interference. An optimum gap exists that trades the SSBI with the image interference. Note that the regular VSSB-OFDM format in [31] is one specific case of the GVSSB-OFDM when the gap is zero.

The experimental setup is shown in Fig. 3.31. The OFDM signal is generated by Matlab program offline and loaded into the 10 Gsam/sec arbitrary waveform generator which functions as a DAC. 136 data subcarriers and the RF tone are zero-padded to an IFFT size of 256. A cyclic prefix of 1/8 of the symbol duration is applied for the margin of synchronization

offsets and the inter-symbol interference (ISI). The data rate is 10 Gbps and the format is 4 QAM. The signal is sent into a recirculating loop containing two EDFA, one span of 80 km SSMF and a 0.6-nm optical bandpass filter (OBF). An optical amplifier is used before the photodiode. The signal is sampled and stored by a 20-Gsam/sec real time scope. The post signal processing including the FFT and iterative detection is implemented offline by Matlab.

3.3.2.3 Experimental Results

By changing the CSPR, the signal performance in terms of the error vector magnitude (EVM) as a function of the gap is shown in Fig. 3.32. The EVM is defined as EVM [%]$= 100 * [\sum_{i=1}^{N} |\bar{d}_i - d_i|^2/N]^{1/2}/|d_{max}|$, where N is the number of the received symbol, d_i and $\bar{d}_i$ are the ideal and received symbols, respectively, and d_{max} is the maximum symbol vector in the constellation diagram. The optimum value is located at 0.35 Gap/BW, where BW is the signal bandwidth. We choose this value for the GVSSB-OFDM and uses zero gap for the regular VSSB-OFDM [31].

The EVM as a function of the CSPR is shown in Fig. 3.33. The results show that the proposed GVSSB format is less sensitive to the CSPR while the regular VSSB format has a higher sensitivity to the CSPR. Because the received CSPR would vary with the number of cascaded optical filters along the optical path, a less sensitivity to the CSPR could mitigate the penalty induced by the filtering effect. The 4-QAM constellations for regular VSSB and GVSSB shown in the inset indicate that the less SSBI allows the GVSSB format has a better signal quality at 10 Gbps. We also measure the EVM versus the iteration number at an OSNR = 15 dB in Fig. 3.34. It shows the required iterations for recovering the data can be reduced for GVSSB-OFDM due to a less SSBI and thus can further simplify the post signal processing.

Figure 3.35 shows the bit error rate (BER) versus the OSNR for the regular VSSB and the proposed GVSSB formats. The CSPR is 4 dB which is optimized for the regular VSSB

format. The input optical power per span is -7 dBm. The results show that the GVSSB has an inherent 1-dB improvement over the regular VSSB due to a less SSBI. After 1600 km uncompensated SSMF transmission, the transmission penalty for GVSSB is only ~ 3 dB while the penalty is up to ~ 10 dB for the regular VSSB. The 8 dB gain of the GVSSB over the regular VSSB format could be attributed to the less sensitivity to the filtering effect of the GVSSB format (less sensitive to CSPR) and the less SSBI which would relax the burden of the iterative reconstruction and cancellation technique at the receiver, especially when the signal is strongly distorted after a long distance transmission.

3.3.2.4 Summary

We experimentally demonstrate a generalized VSSB-OFDM format that judiciously determines the frequency gap between an inserted RF tone and the signal. The proposed scheme for 10 Gbps exhibits ~3 dB penalty after 1600 km SSMF transmission, and has an 8 dB improvement over the regular VSSB-OFDM.

References

[1] B. J. C. Schmidt et al, “OFC’07, paper PDP 18.

[2] W. Shieh, “PMD-Supported Coherent Optical OFDM Systems,” *IEEE Photon. Technol. Lett.*, vol. 19, pp. 134-136, 2007.

[3] D. F. Hewitt, “Orthogonal Frequency Division Multiplexing using Baseband Optical Single Sideband for Simpler Adaptive Dispersion Compensation,”OFC’07, paper OME7.

[4] W. R. Peng et al, “Improving the Transmission Performance for an Externally Modulated Baseband Single Sideband OFDM Signal Using Nonlinear Post-compensation and Differential Encoding Schemes,” ECOC’07, paper P078.

[5] M. Schuster et al, “Spectrally efficient OFDM-transmission with compatible single-sideband modulation for direct detection,” ECOC’07, paper P075.

[6] M. Schuster et al, “Spectrally Efficient Compatible Single-Sideband Modulation for OFDM Transmission with Direct Detection,” Photon. Technol. Lett., vol. 20, pp. 670- 672, 2008.

[7] B. J. C. Schmidt et al., “Experimental Demonstrations of Electronic Dispersion Compensation for Long-Haul Transmission Using Direct-Detection Optical OFDM,” IEEE J. Lightwave Technol., vol. 26, pp. 196-203, 2008.

[8] C. Xie, “PMD Insensitive Direct-Detection Optical OFDM Systems Using Self-Polarization Diversity,” OFC’08 paper OMM2.

[9] W. R. Peng et al., “Experimental Demonstration of 340 km SSMF Transmission Using a Virtual Single Sideband OFDM Signal that Employs Carrier Suppressed and Iterative Detection Techniques,” OFC’08 paper OMU1.

[10] W. R. Peng et al., “Experimental Demonstration of a Coherently Modulated and Directly Detected Optical OFDM System Using an RF-Tone Insertion,” OFC’08 paper OMU2.

[11] G. Xing et al., “Frequency offset and I/Q imbalance compensation for direct-conversion receivers”IEEE Trans. Wireless Comm., vol. 4, pp. 673-680 , 2005.

[12] D. Qian et al, ”8×11.5-Gb/s OFDM Transmission over 1000km SSMF using Conventional DFB Lasers and Direct Detection,” OFC’08, paper OMM3.

[13] B. Huettl et al,”320 Gbit/s DQPSK All-Optical Wavelength Conversion using Periodically Poled LiNbO3,” CLEO’07, paper CThF1.

[14] H. Furukawa et al, ” Tunable All-Optical Wavelength Conversion of 160-Gb/s RZ Optical Signals by Cascaded SFG-DFG Generation in PPLN Waveguide,” Photon. Technol. Lett., vol. 19, pp. 384-386, 2007.

[15] L. Christen et al, ”Tunable 105-ns Optical Delay for 80-Gbit/s RZ-DQPSK, 40-Gbit/s RZ-DPSK, and 40-Gbit/s RZ-OOK Signals using Wavelength Conversion and Chromatic Dispersion,” OFC’08, paper OTuD1.

[16] A. J. Lowery et al., “Performance of Optical OFDM in Ultralong-Haul WDM Lightwave Systems,” J. Lightwave Technol., vol. 25, pp. 131-138, 2007.

[17] W. R. Peng et al., “Experimental Demonstration of 340 km SSMF Transmission Using a Virtual Single Sideband OFDM Signal that Employs Carrier Suppressed and Iterative Detection Techniques,” OFC’08 paper OMU1.

[18] W. R. Peng et al., “Experimental Demonstration of a Coherently Modulated and Directly Detected Optical OFDM System Using an RF-Tone Insertion,” OFC’08 paper OMU2.

[19] A. J. Lowery et al., *IEEE J. Lightwave Technol.*, vol. 25, pp. 131-138, 2007.

[20] M. Mayrock et al, “PMD tolerant direct-detection optical OFDM system,” ECOC’07 paper Tu. 5.2.5.

[21] Lajos Hanzo et al., Single- and Multi-Carrier Quadrature Amplitude Modulation. Wiley, Chichester, 2nd edition, 2000.

[22] A. J. Lowery et al, “Orthogonal frequency division multiplexing for adaptive dispersion compensation in long-haul WDM systems,” OFC’06 paper PDP39.

[23] M. Mayrock et al, “PMD tolerant direct-detection optical OFDM system,” ECOC’07 paper Tu. 5.2.5.

[24] B. J. C. Schmidt et al, “Experimental demonstrations of 20 Gb/s direct-detection optical OFDM and 12Gb/s with a colorless transmitter,” OFC’07, paper PDP 18.

[25] D. F. Hewitt, “Orthogonal frequency division multiplexing using baseband optical single sideband for simpler adaptive dispersion compensation,” OFC’07, paper OME7.

[26] W. R. Peng et al, “Improving the transmission performance for an externally modulated baseband single sideband OFDM signal using nonlinear post-compression and differential encoding schemes,” ECOC’07 paper P078.

[27] M. Schuster et al, “Spectrally efficient OFDM-transmission with compatible single sideband modulation for direct detection,” ECOC’07 paper P075.

[28] F. Buchali et al, “Optimization of an optical OFDM system by peak to average signal ratio reduction,” ECOC’07, Paper Tu. 5.2.4.

[29] B. J. C. Schmidt et al.,” Experimental Demonstrations of Electronic Dispersion Compensation for Long-Haul Transmission Using Direct-Detection Optical OFDM**,”** IEEE Journal of Lightwave. Technol., pp. 196, 2008.

[30] C. Xie, “PMD Insensitive Direct Detection Optical OFDM Systems Using Self-Polarization Diversity,” OFC’08 paper OMM2.

[31] W. R. Peng et al., “Experimental Demonstration of 340 km SSMF Transmission Using a Virtual Single Sideband OFDM Signal that Employs Carrier Suppressed and Iterative Detection Techniques,” OFC’08 paper OMU1.

[32] W. R. Peng et al., “Experimental Demonstration of a Coherently Modulated and Directly Detected Optical OFDM System Using an RF-Tone Insertion,” OFC’08 paper OMU2.

[33] S. L. Jansen et al., “Pre-Emphasis and RF-Pilot Tone Phase Noise Compensation for Coherent OFDM Transmission Systems” LEOS’07 paper MA 1.2.

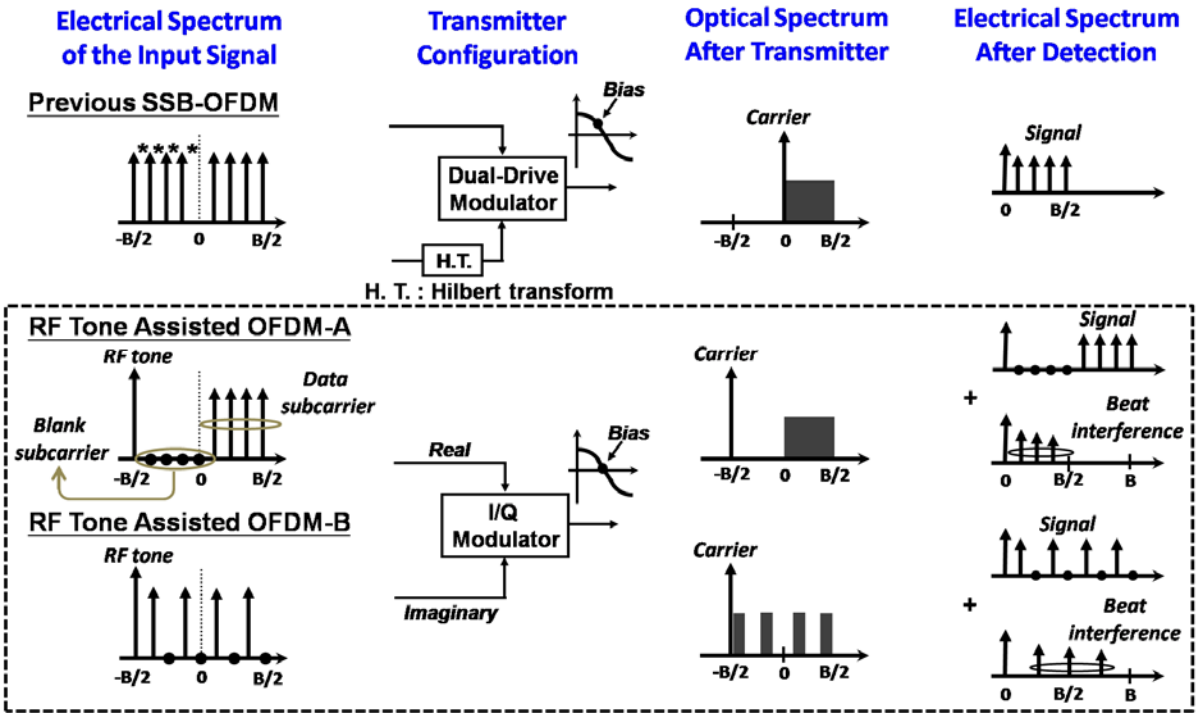

Fig. 3.1 Operation principles for (a) the conventional power-modulated SSB-OFDM, and (b) the proposed RF-tone assisted OFDM-A (gapped) and OFDM-B (interleaved).

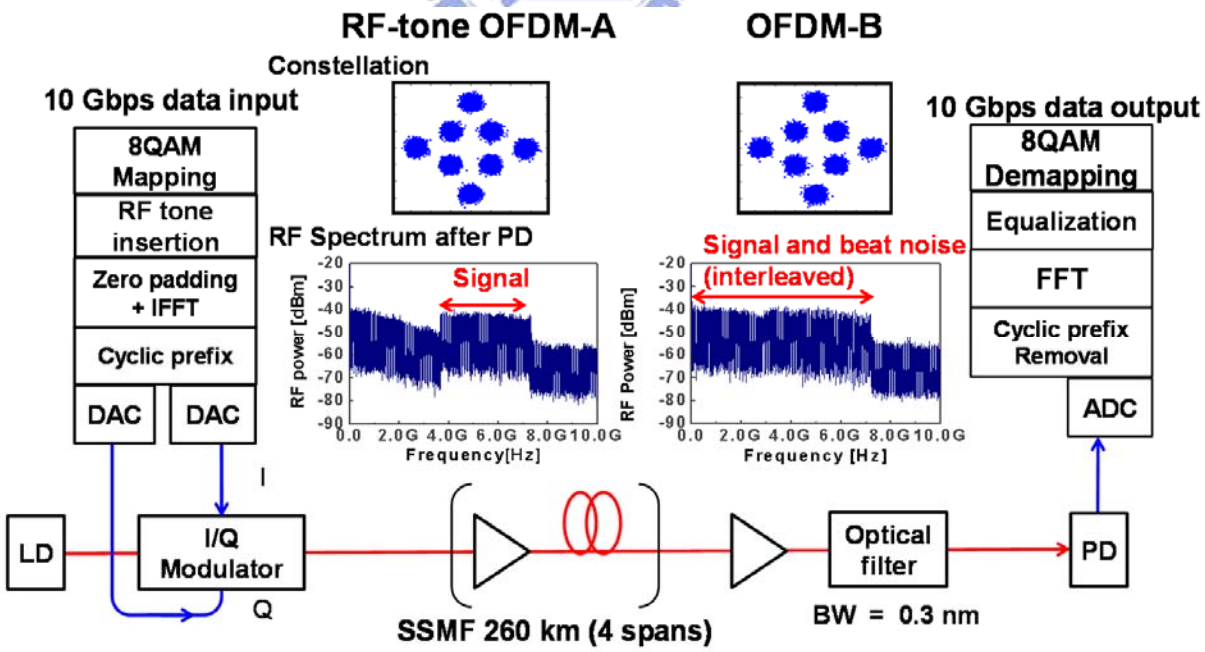

Fig. 3.2 Experimental setup of the RF-tone assisted OFDM.

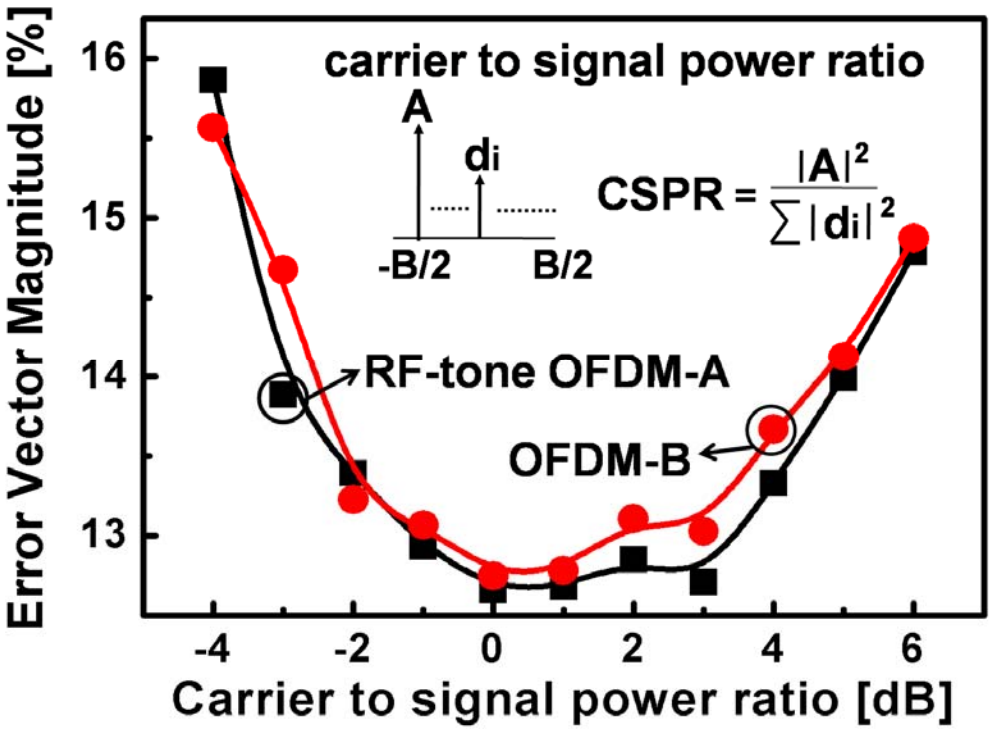

Fig. 3.3 Experimental results of error vector magnitude versus the carrier to signal power ratio.

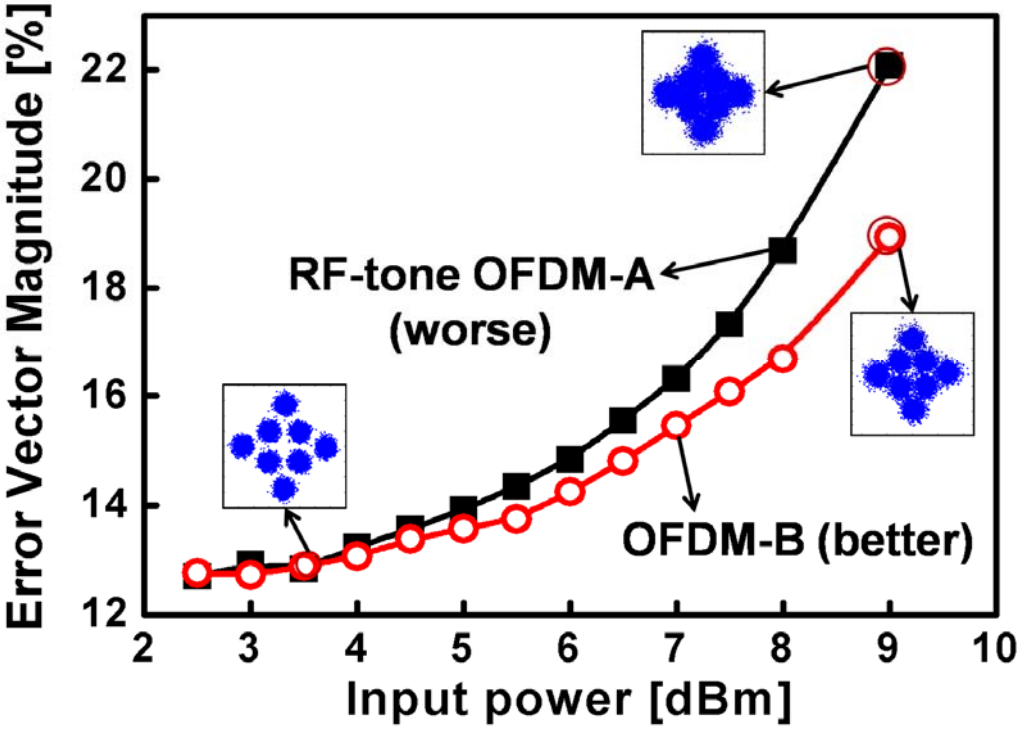

Fig. 3.4 Experimental results of error vector magnitude versus the input power per span.

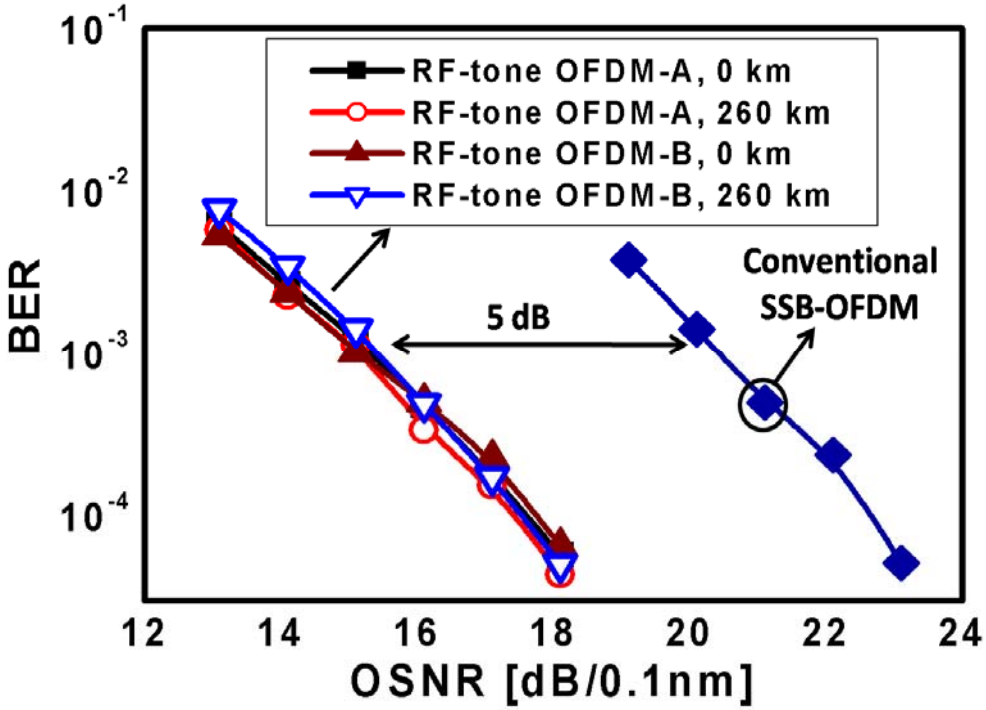

Fig. 3.5 Experimental results of BER versus OSNR.

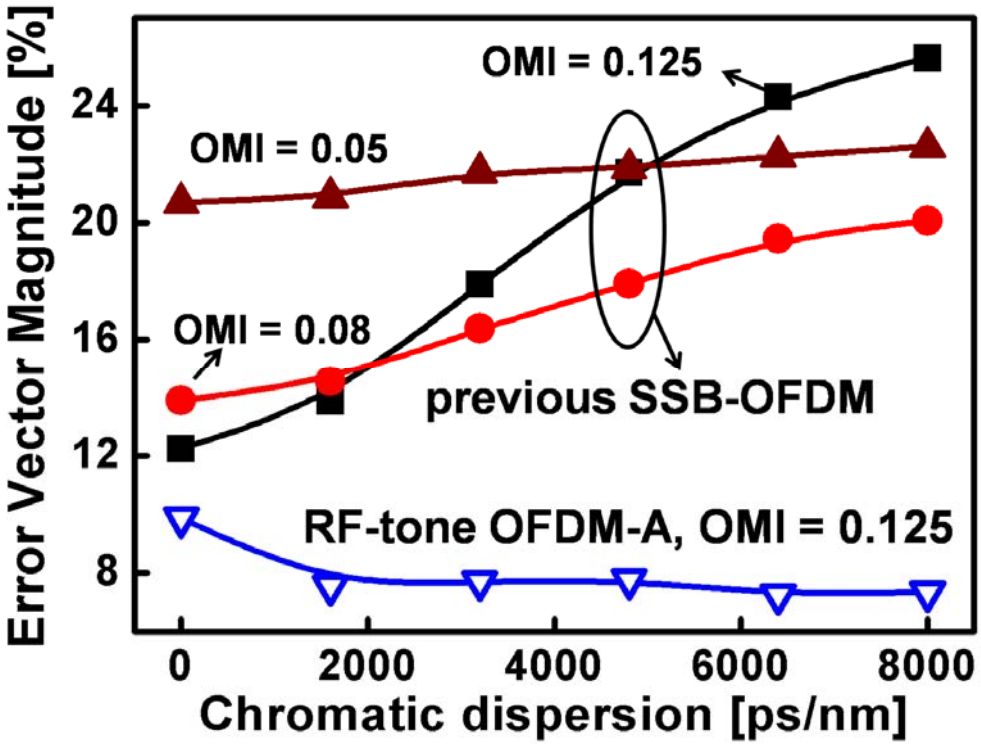

Fig. 3.6 Simulation of the error vector magnitude as a function of the chromatic dispersion.

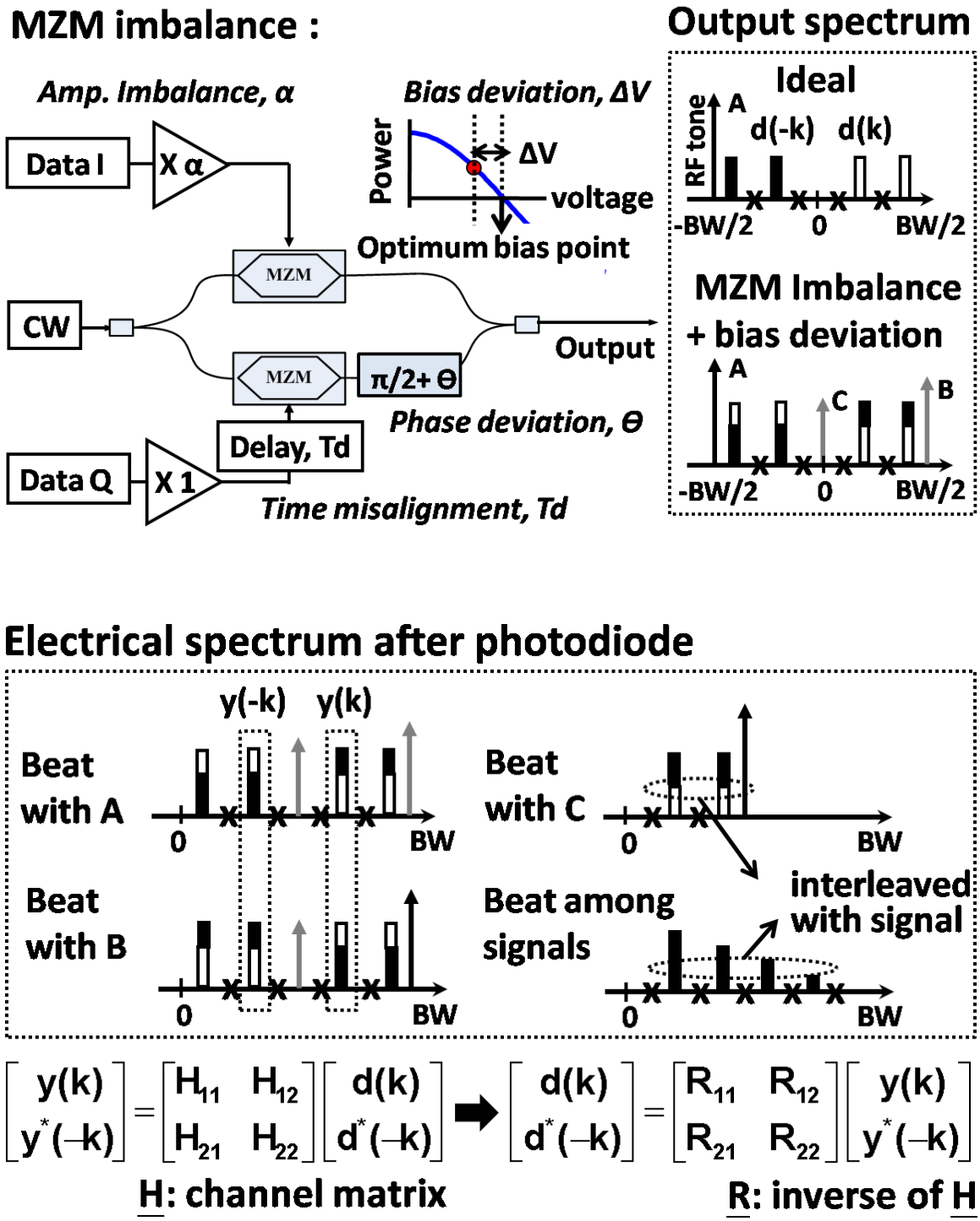

Fig. 3.7 (a) The MZM imbalance and bias deviation, and the corresponding output spectrum of the RF-tone assisted OFDM, (b) the interfered signals after photodiode and the proposed 2x2 equalization matrix compensating the imbalance effects.

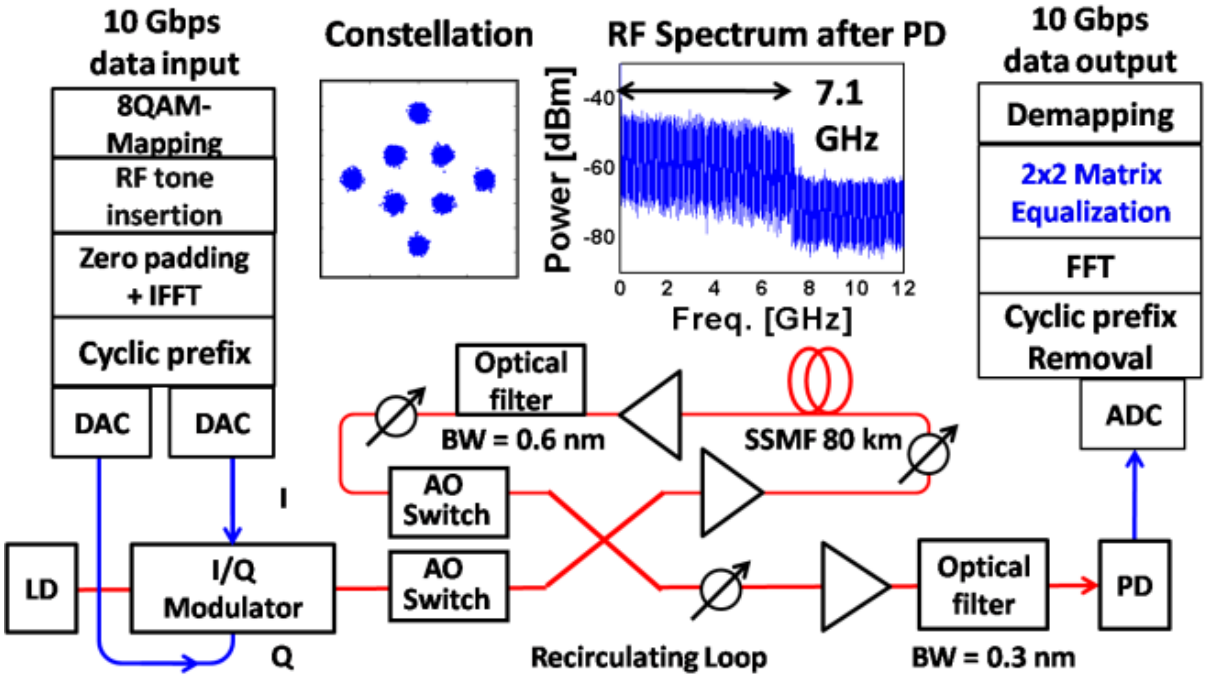

Fig. 3.8 Experimental setup of the joint equalization technique for MZM imbalance and fiber CD.

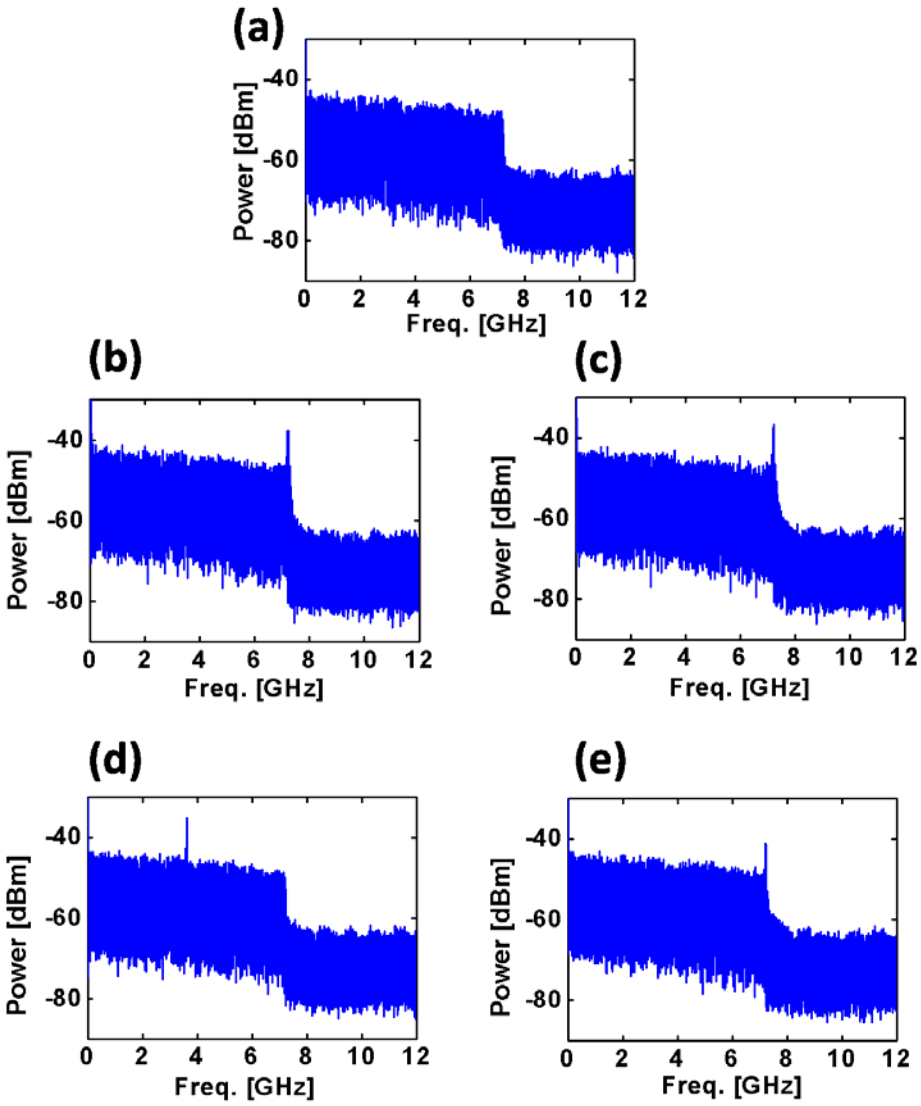

Fig. 3.9 Measured RF spectra after PD, (a) ideal operation, (b) with a amplitude imbalance of $\alpha = 1.38$, (c) with a phase deviation of $0.1\ \pi$, (d) with a bias deviation of $\Delta V / Vrms$, where Vrms is the root-mean square of the input signal, (e) with a time misalignment of Td = 10 ps.

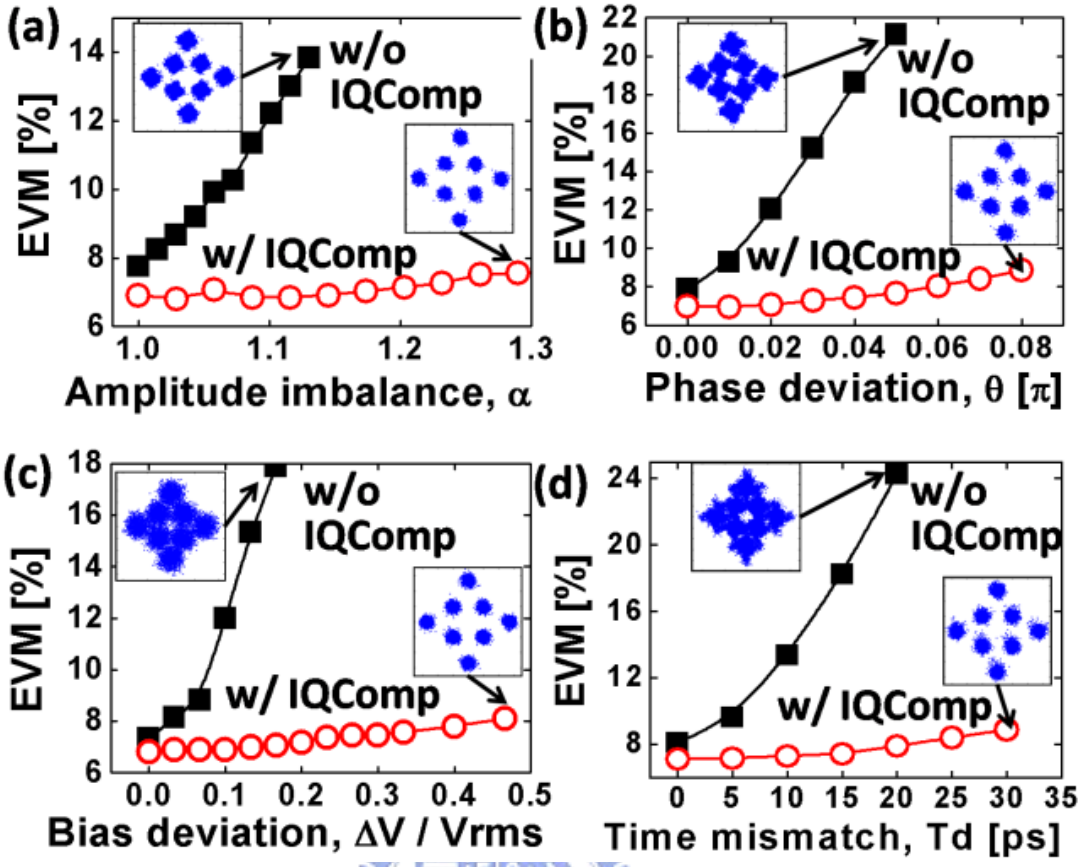

Fig. 3.10 EVM versus amplitude imbalance, (b) EVM versus phase deviation, (c) EVM versus bias deviation, where Vrms is the root-mean square of the input signal, (d) EVM versus the time misalignment.

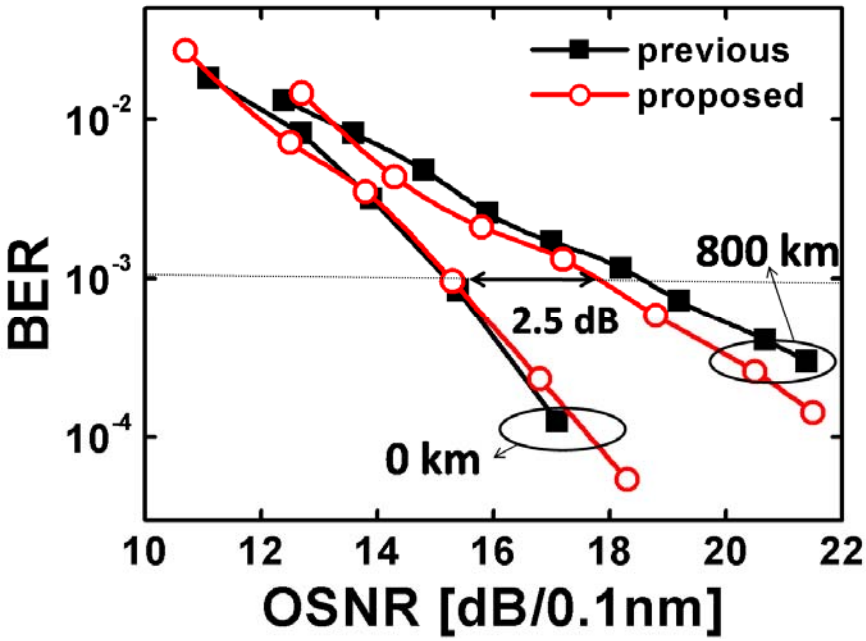

Fig. 3.11 Bit error rate (BER) versus the optical signal to noise ratio (OSNR) for without and without I/Q compensation scheme, before and after 800 km uncompensated transmission. Note that there is no I/Q imbalance for this plot.

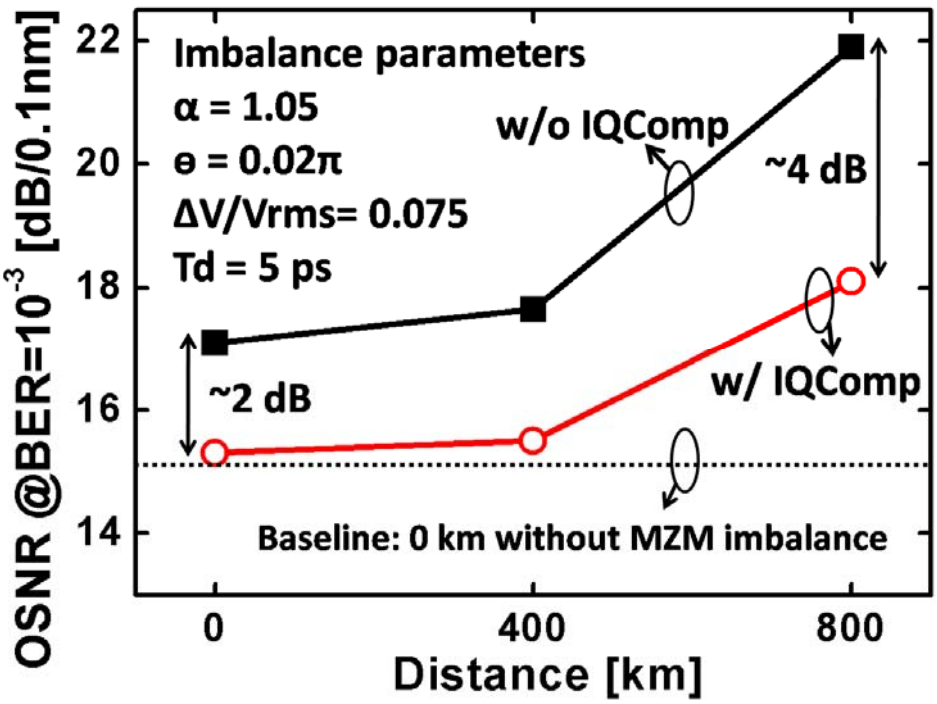

Fig. 3.12 Required OSNR (0.1 nm) for BER = 10^{-3} versus the fiber distance with MZM imbalance.

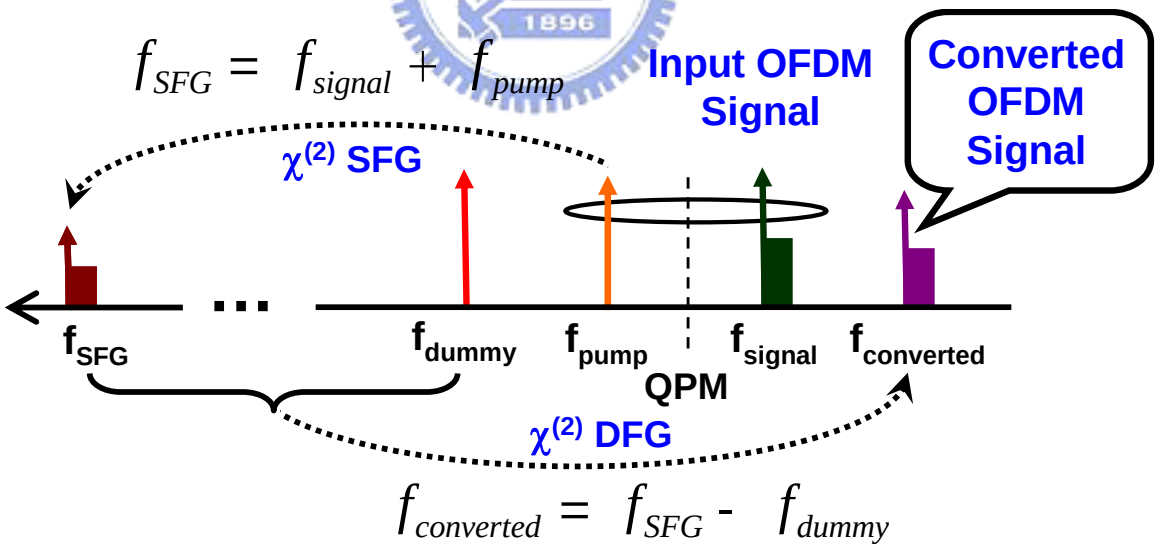

Fig. 3.13 Concept of wavelength conversion using SFG/DFG in a PPLN waveguide.

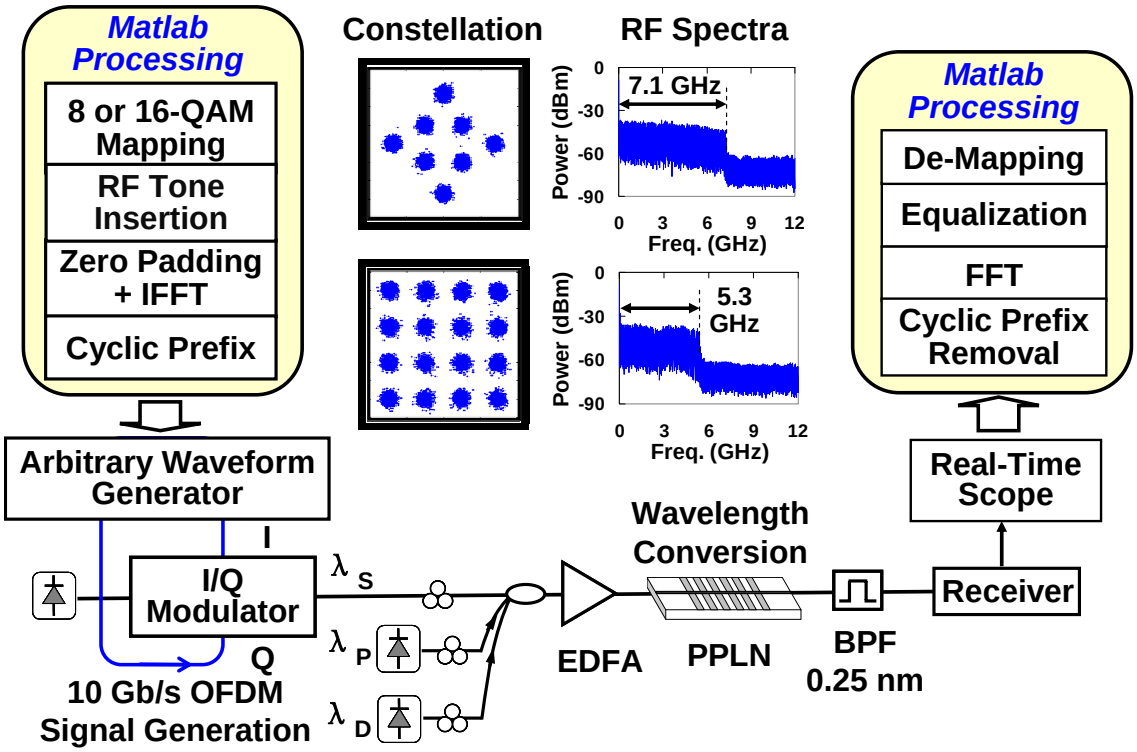

Fig. 3.14 Experimental setup of OFDM wavelength conversion. The constellation and RF spectra of 8 & 16-QAM are inserted.

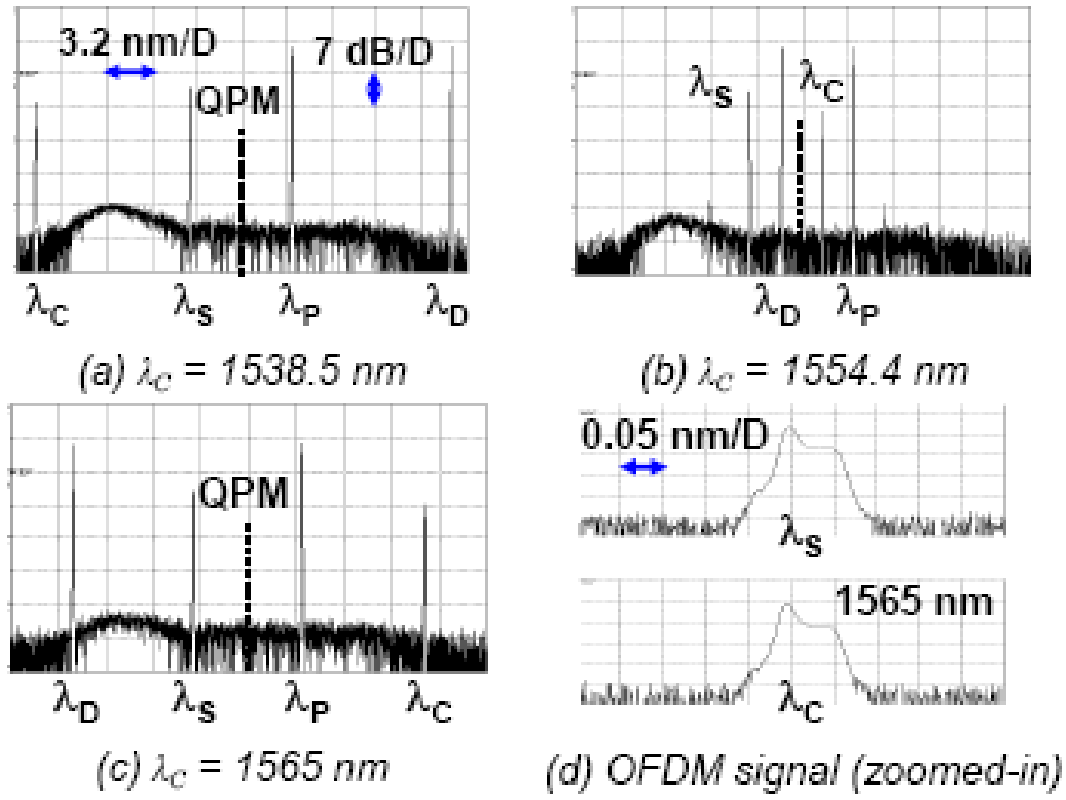

Fig. 3.15 Optical spectra after wavelength conversion. QPM: quasi-phase matching wavelength.

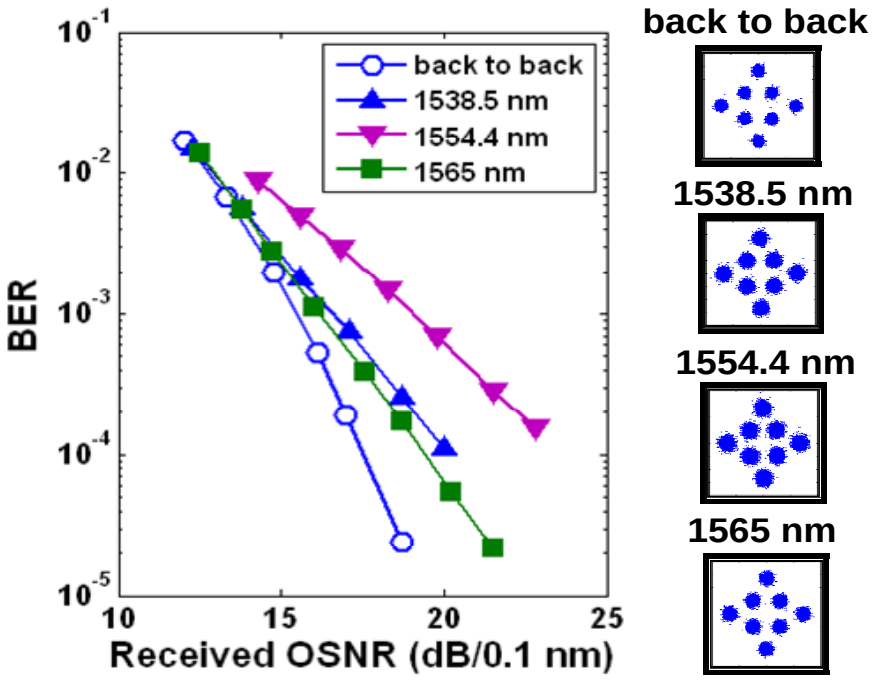

Fig. 3.16 BER performance of the 10 Gb/s RF-tone assisted OFDM signal for both back to back and after conversion.

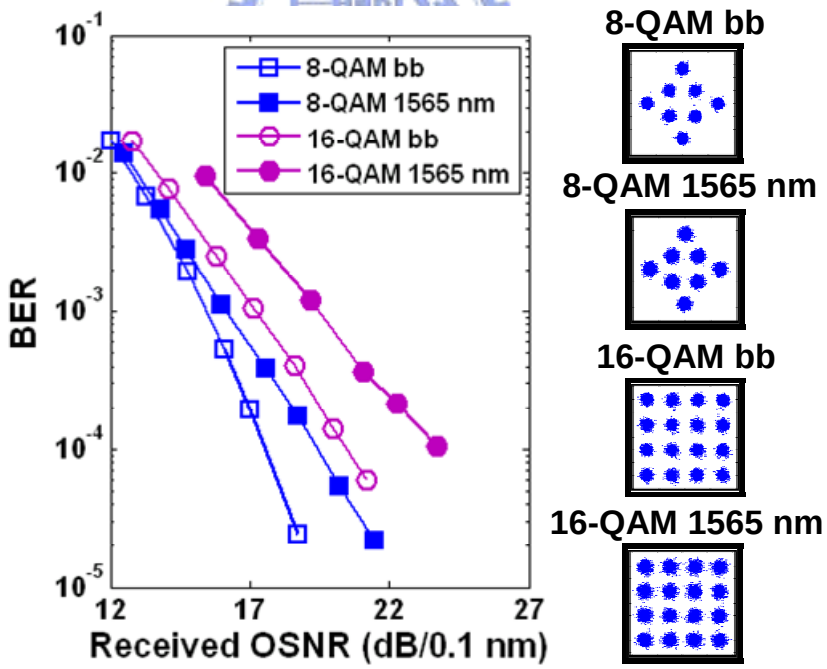

Fig. 3.17 BER performance of 8-QAM and 16-QAM for both back to back (bb) and after wavelength conversion.

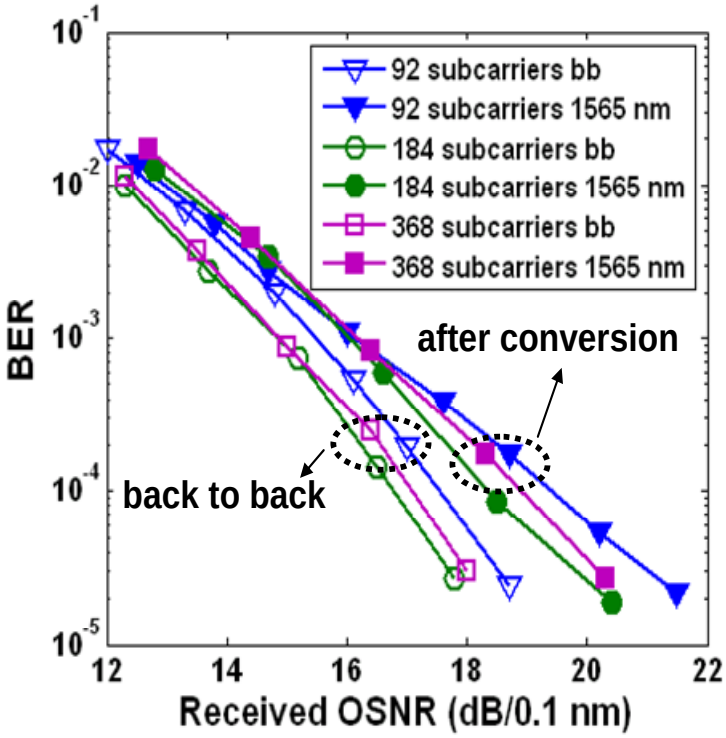

Fig. 3.18 BER with different subcarrier numbers.

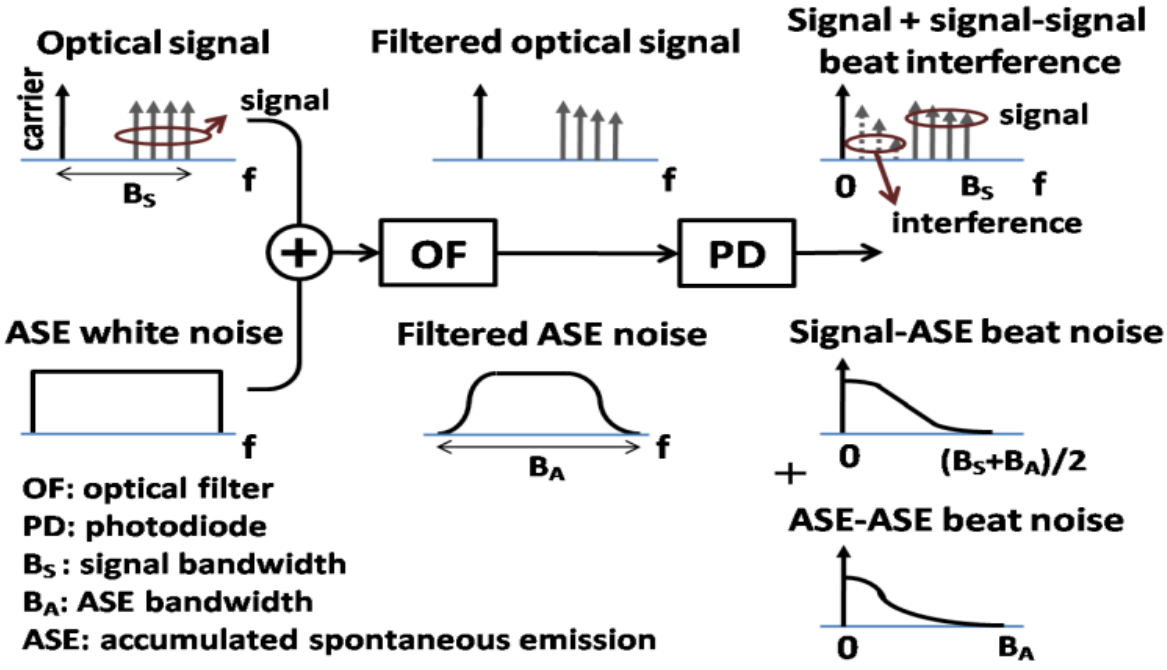

Fig. 3.19 The progress of the power spectra of the SSB-OFDM signal and the ASE noise before and after the photodiode.

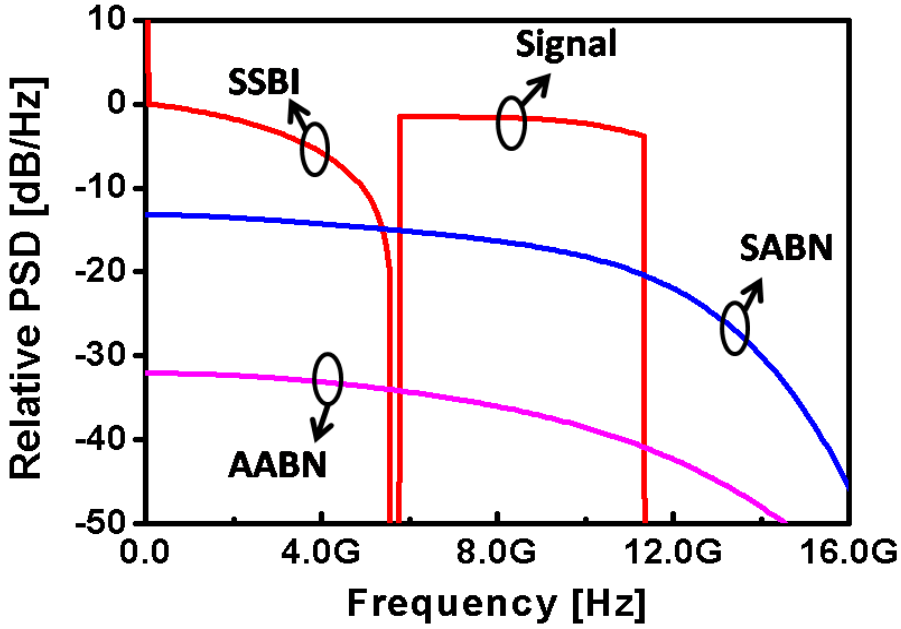

Fig. 3.20 Simulated electrical power spectra of the OFDM signal, the signal-signal beat interference (SSBI), the colored signal-

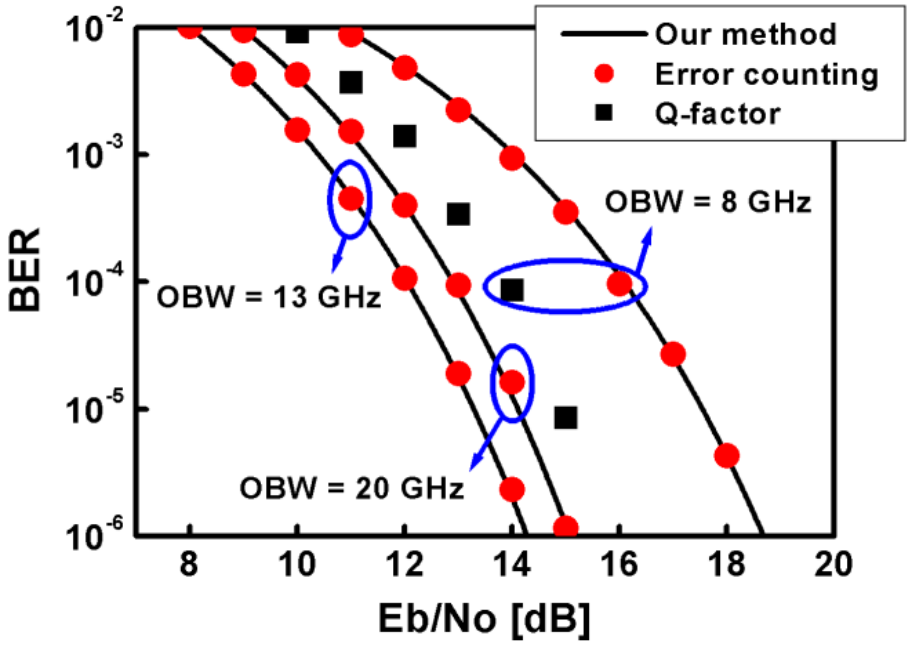

Fig. 3.21 BER versus OSNR with different optical filter bandwidth (OBW). The data rate is 10 Gbps with 4-QAM. The OFDM bandwidth is ~11.8 GHz. The Q-factor is extracted from all the received constellation points.

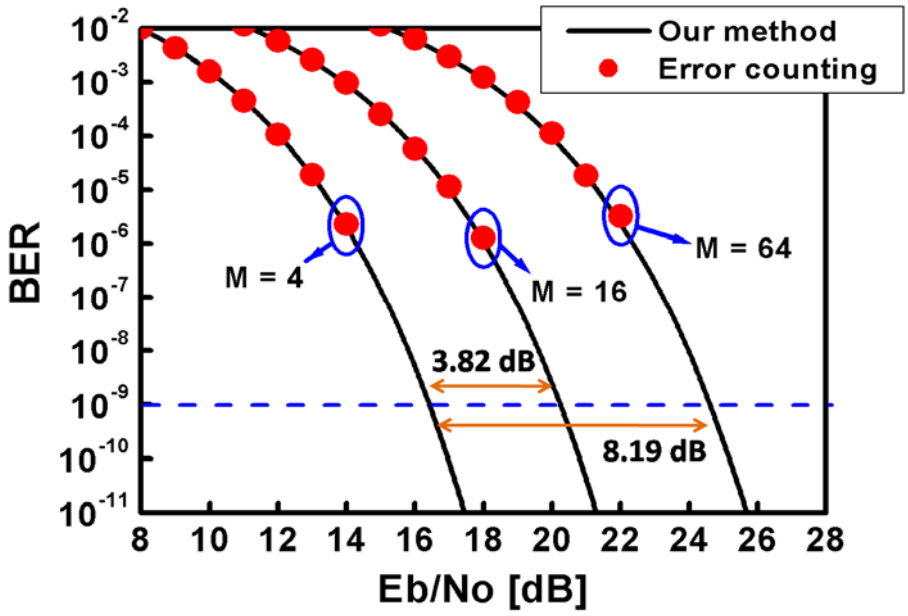

Fig. 3.22 BER versus OSNR with different OFDM QAM formats. The optimum optical bandwidths for 4-, 16- and 64-QAM 10-Gbps SSB-OFDM signals are 13, 6.7 and 4.6 GHz.

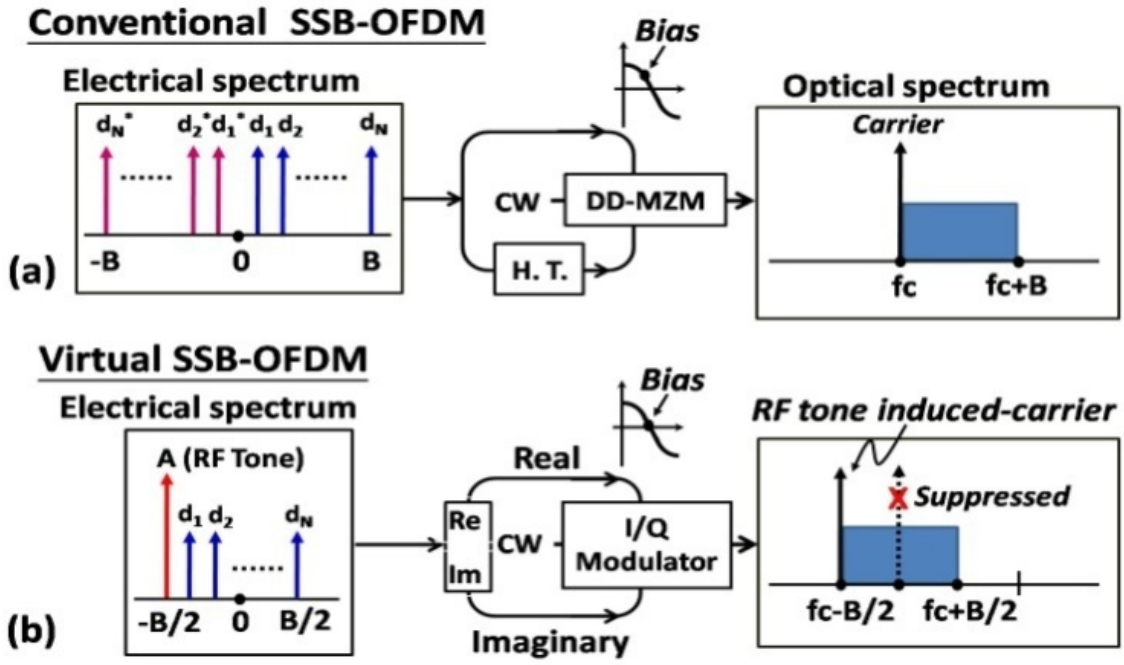

Fig. 3.23 Transmitter architectures for the (a) conventional SSB-OFDM and (b) the proposed virtual SSB-OFDM. (H. T.: Hilbert Transform)

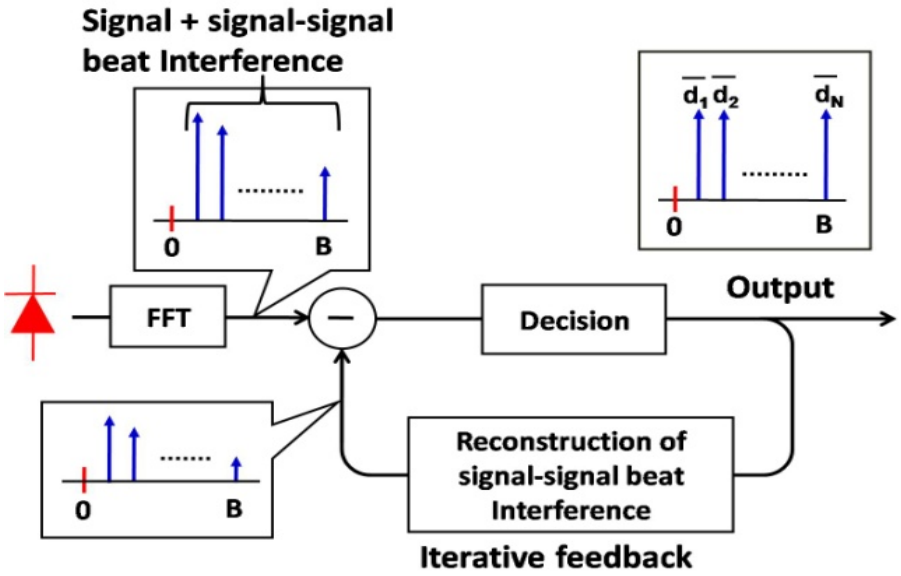

Fig. 3.24 Iterative detection for the virtual SSB-OFDM.

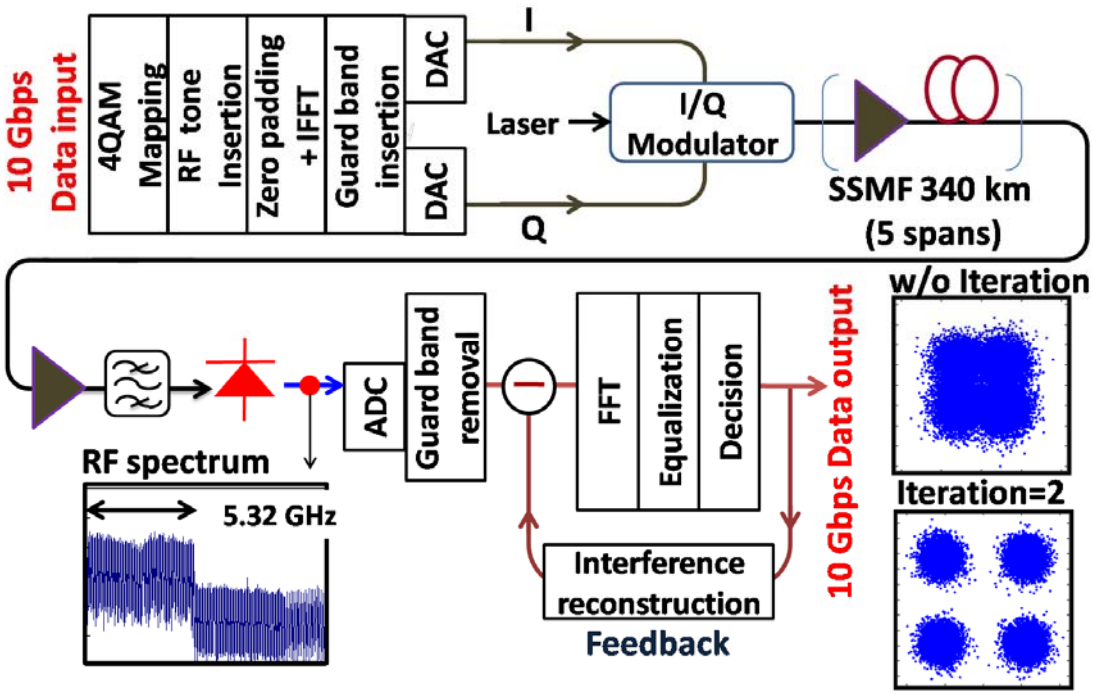

Fig. 3.25 Experimental setup of the virtual SSB-OFDM.

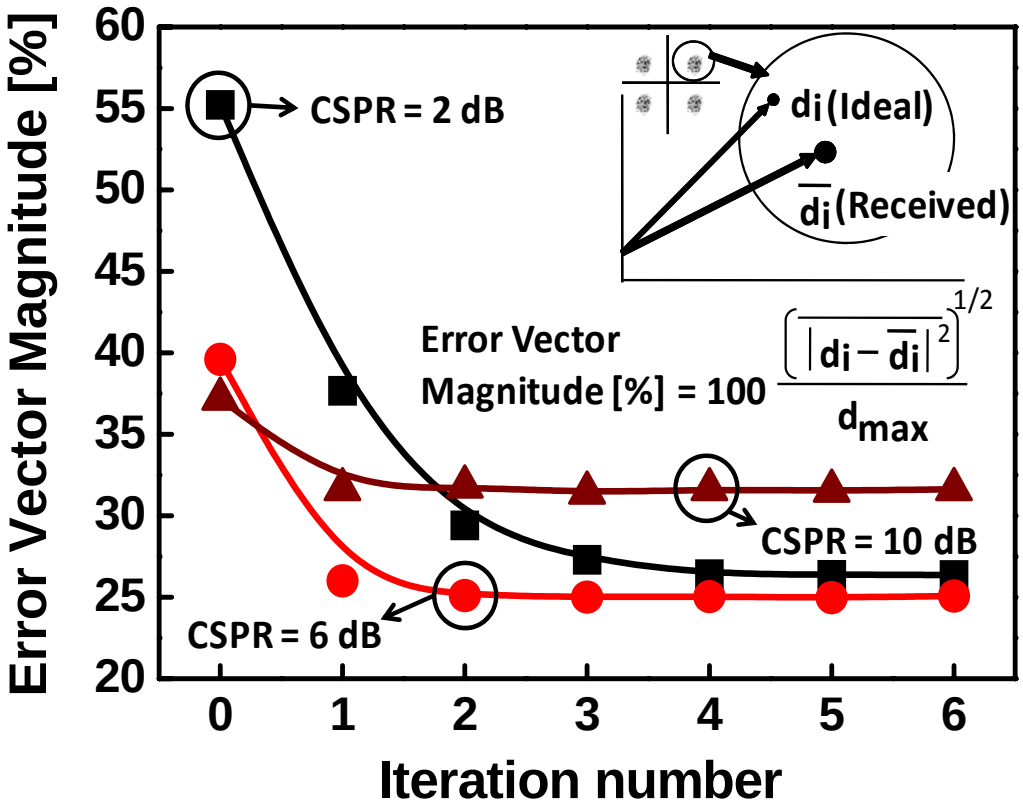

Fig. 3.26 Measured error vector magnitude (EVM) versus the receiver iteration numbers.

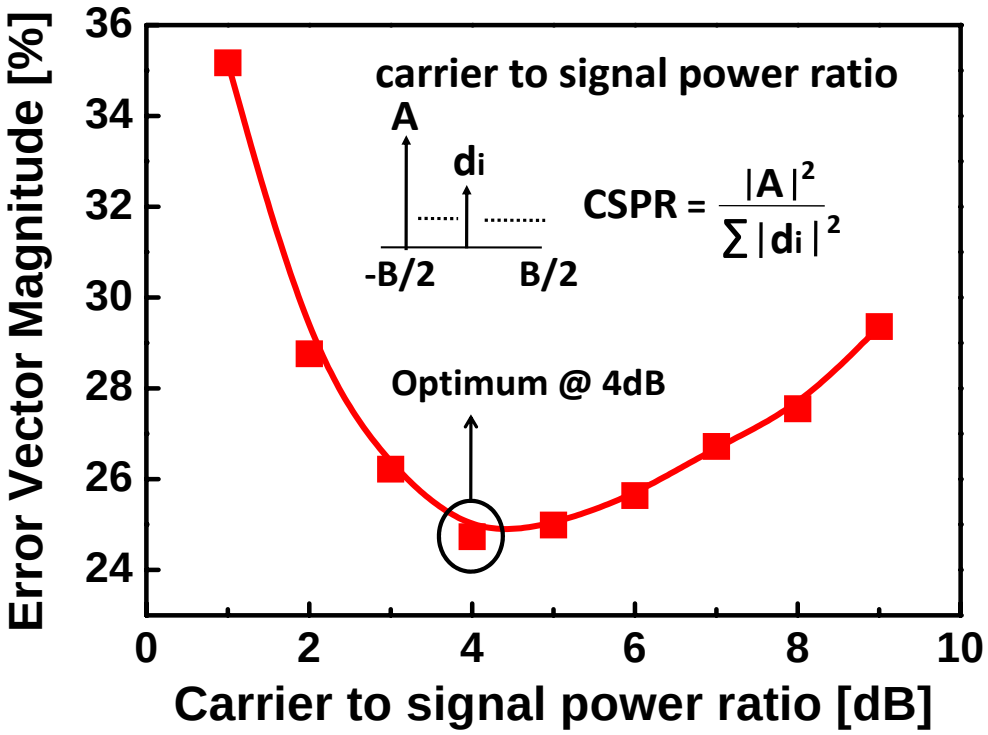

Fig. 3.27 Measured EVM versus the carrier to signal power ratio (CSPR).

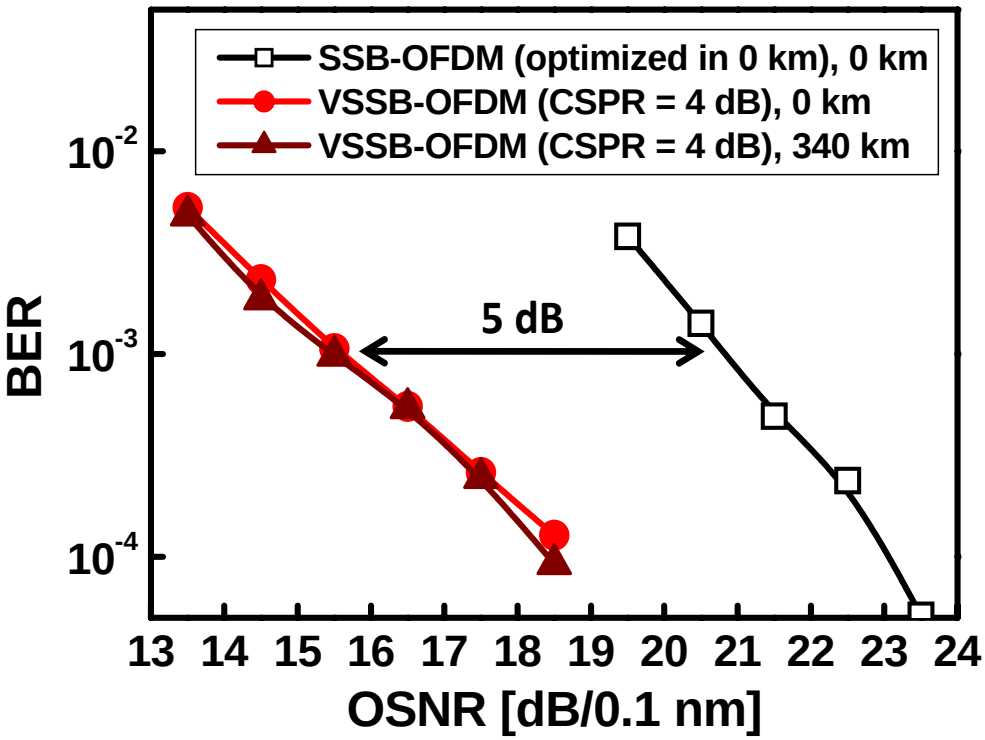

Fig. 3.28 Measured bit error rate versus the optical signal to noise ratio for the conventional and the virtual SSB-OFDM.

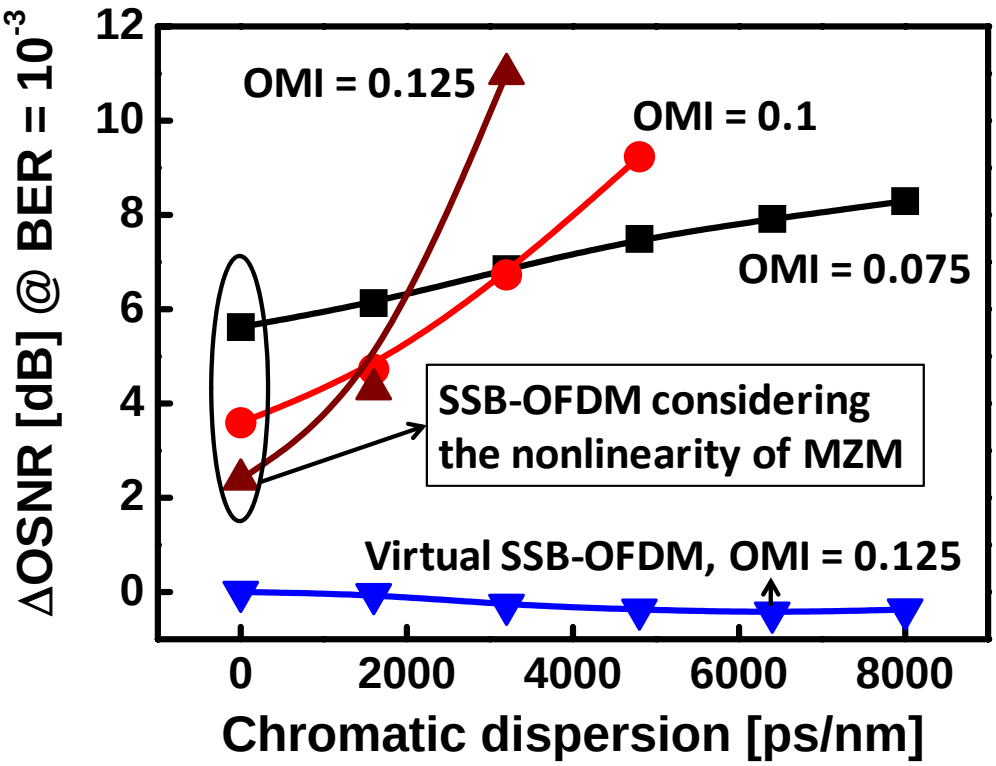

Fig. 3.29 Simulated results for the conventional and the virtual SSB-OFDM. OMI (optical modulation index) is defined as [Vin]rms/Vπ, where [Vin]rms is the root-mean square of the electrical input to the MZM and Vπ is the switching voltage of the MZM.

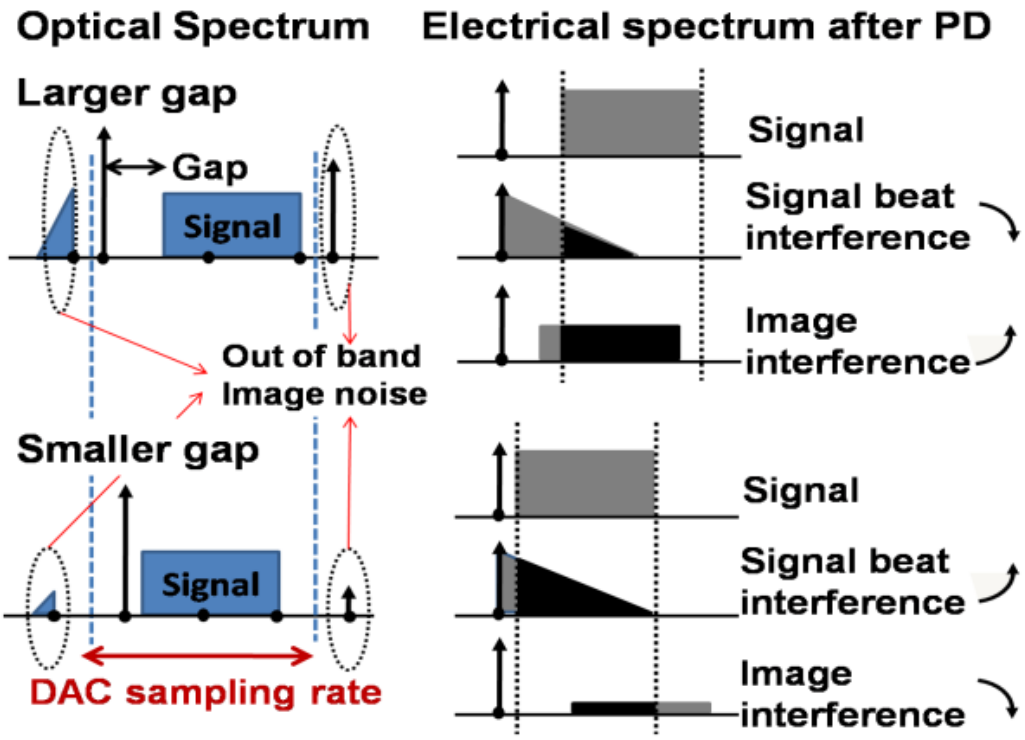

Fig. 3.30 The proposed generalized VSSB-OFDM (GVSSB-OFDM) with tunable gap. The optimum gap trades the signal-signal beat interference (SSBI) with the image interference.

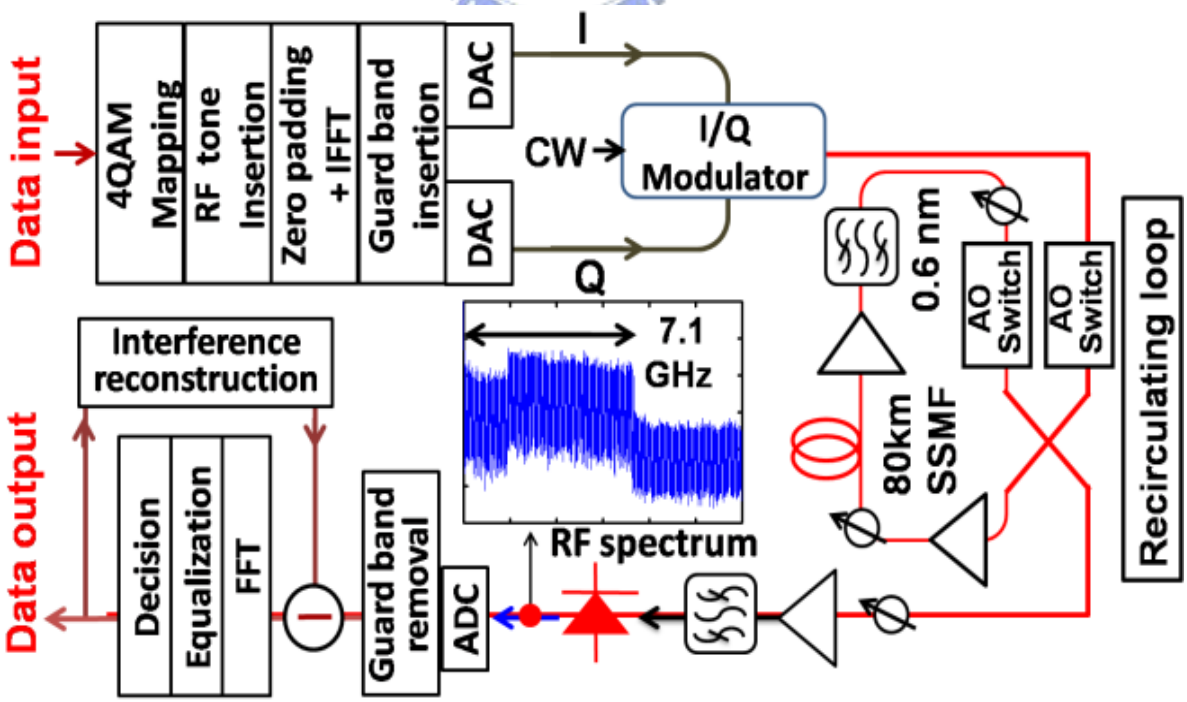

Fig. 3.31 Experimental setup for GVSSB-OFDM system.

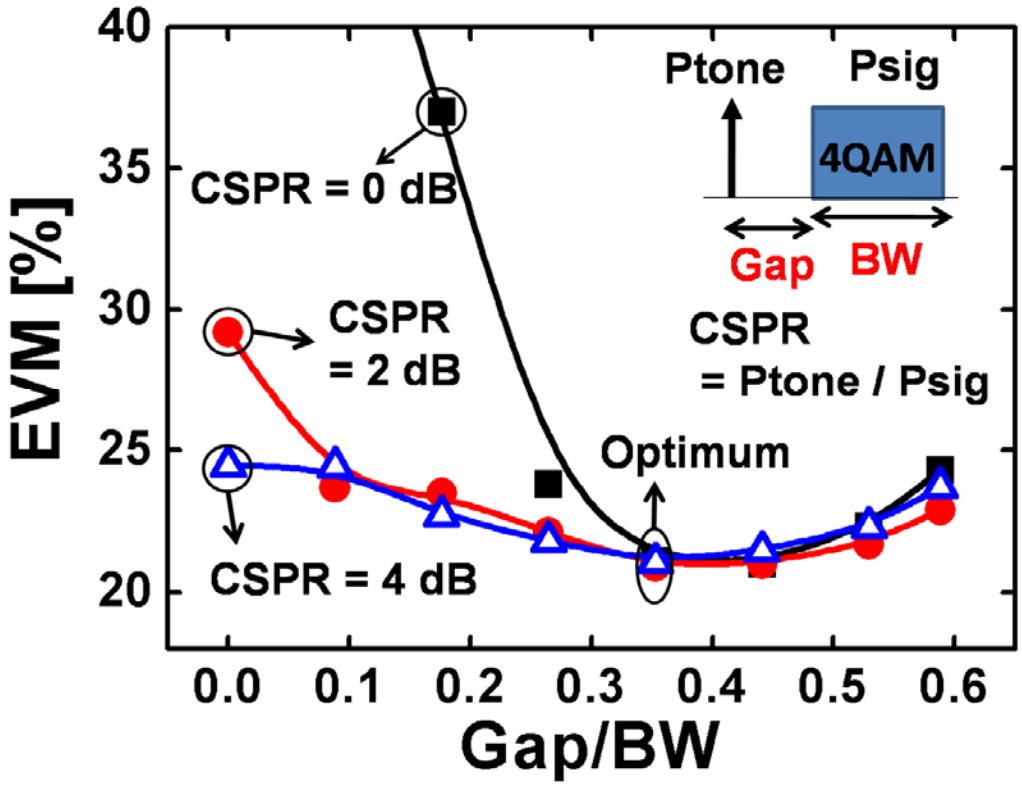

Fig. 3.32 Measured EVM versus the frequency gap for different values of CSPR.

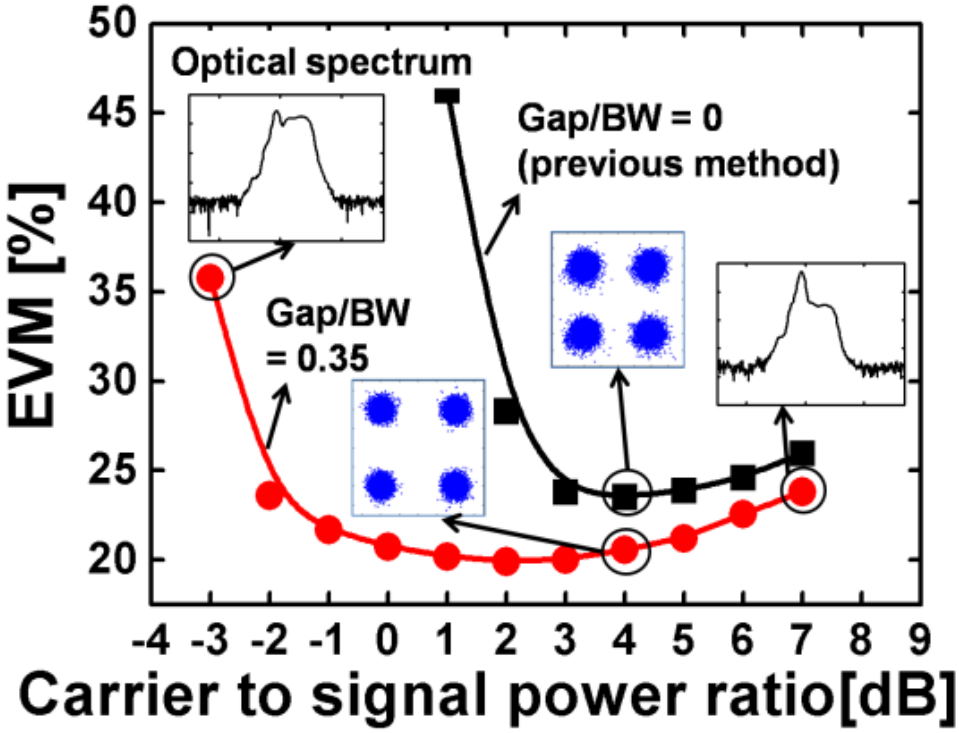

Fig. 3.33 Measured EVM versus the carrier to signal power ratio.

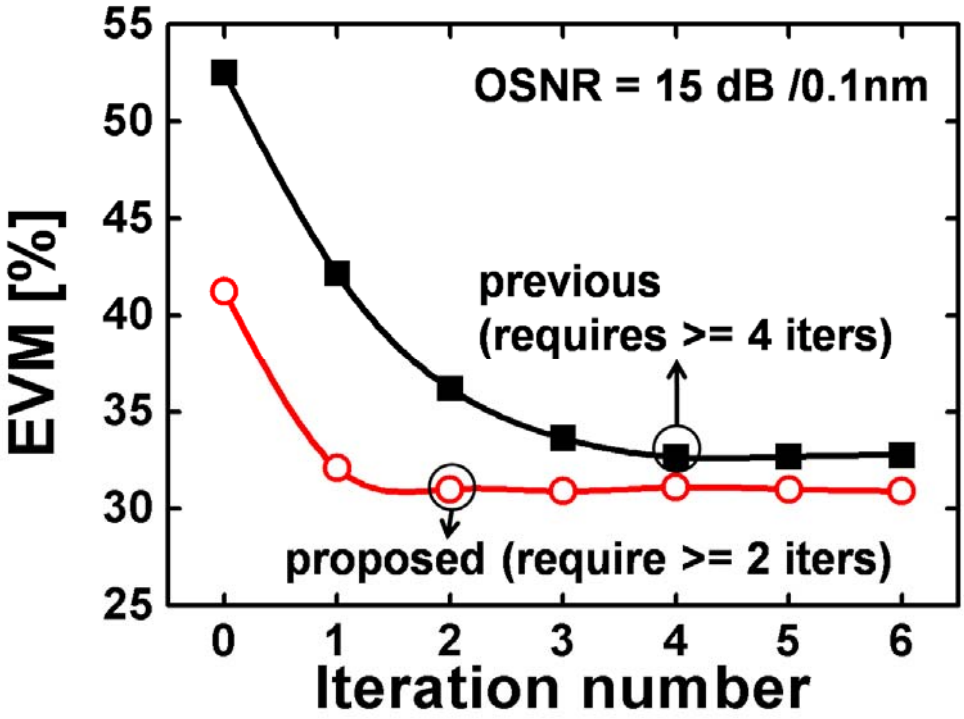

Fig. 3.34 Measured EVM verus the iteration number.

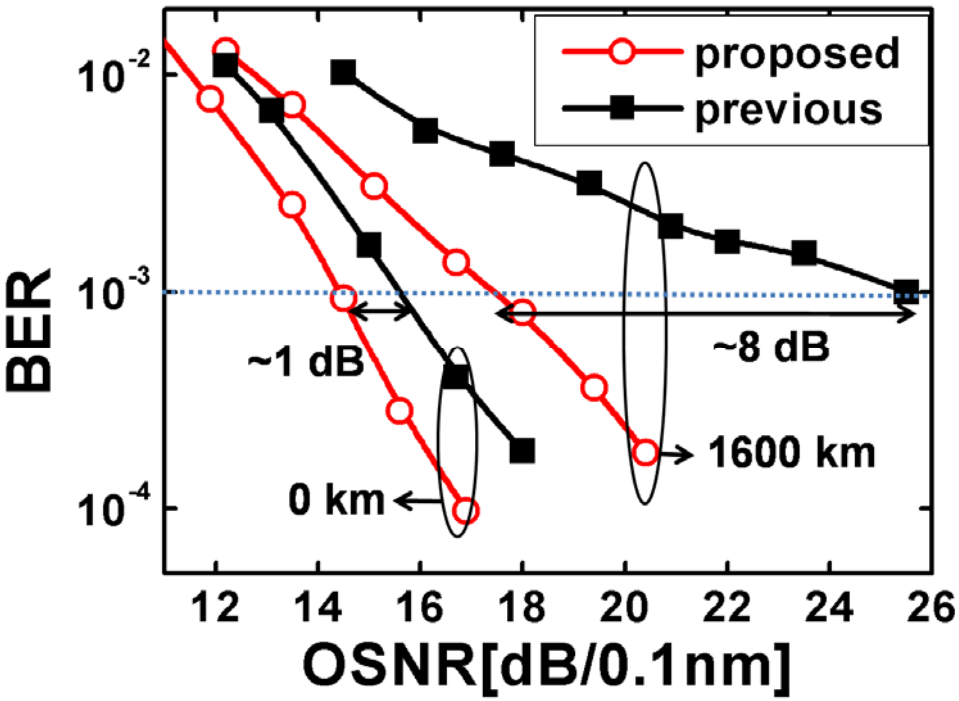

Fig. 3.35 Measured BER versus the OSNR.